Journal of Geophysical Research: Oceans

RESEARCH ARTICLE
10.1029/2018JC013828

SIDDIES Corridor: A Major East-West Pathway of Long-Lived Surface and Subsurface Eddies Crossing the Subtropical South Indian Ocean

A. F. Dilmahamod[1,2,3], B. Aguiar-González[4,5], P. Penven[2], C. J. C. Reason[1], W. P. M. De Ruijter[6], N. Malan[1,3,7], and J. C. Hermes[1,3,8]

[1]Department of Oceanography, University of Cape Town, Cape Town, South Africa, [2]Univ. Brest, CNRS, IRD, Ifremer, Laboratoire d'Oceanographie Physique et Spatial (LOPS), IUEM, Brest, France, [3]South African Environmental Observation Network, Egagasini Node, Roggebaai, South Africa, [4]NIOZ Royal Netherlands Institute for Sea Research, Department of Ocean Systems Sciences, Utrecht University, AB Den Burg, Texel, The Netherlands, [5]School of Marine Science and Policy College of Earth, Ocean and Environment, University of Delaware, Newark, Delaware, USA, [6]Institute for Marine and Atmospheric Research, Utrecht University, CC Utrecht, The Netherlands, [7]Department of Oceanography, Nansen-Tutu Centre for Marine Environmental Research, University of Cape Town, Cape Town, South Africa, [8]Nelson Mandela University, Port Elizabeth, South Africa

Key Points:
- Presence of a SIDDIES (South Indian Ocean Eddies) corridor linking the eastern to the western basin
- Anticyclonic as well as cyclonic subSIDDIES occur in the South Indian Ocean
- Subsurface-intensified eddies (subSIDDIES) play a major role in the heat/freshwater fluxes

Correspondence to:
A. Fehmi Dilmahamod,
fehmi.dilmahamod@gmail.com

Citation:
Dilmahamod, A. F., Aguiar-González, B., Penven, P., Reason, C. J. C., De Ruijter, W. P. M., Malan, N., & Hermes, J. C. (2018). SIDDIES corridor: A major east-west pathway of long-lived surface and subsurface eddies crossing the subtropical south indian ocean. *Journal of Geophysical Research: Oceans*, *123*. https://doi.org/10.1029/2018JC013828

Received 23 JAN 2018
Accepted 7 MAY 2018
Accepted article online 16 MAY 2018

Abstract South Indian Ocean eddies (SIDDIES), originating from a high evaporation region in the eastern Indian Ocean, are investigated by tracking individual eddies from satellite data and co-located Argo floats. A subsurface-eddy identification method, based on its steric dynamic height anomaly, is devised to assign Argo profiles to surface eddies (surfSIDDIES) or subsurface eddies (subSIDDIES). These westward-propagating, long-lived features (>3 months) prevail over a preferential latitudinal band, forming a permanent structure linking the eastern to the western Indian Ocean, that we call the 'SIDDIES Corridor'. Key features have been revealed in the mean thermohaline vertical structure of these eddies. Anticyclonic SIDDIES are characterized by positive subsurface salinity anomalies, with subSIDDIES not exhibiting negative surface anomalies, as opposed to surfSIDDIES. Cyclonic subSIDDIES also occur, but their related salinity anomalies are weaker. SubSIDDIES exhibit two cores of different temperature polarities in their surface and subsurface levels. Cyclonic subSIDDIES have their cores at around 150-200 m depth along the 25.4-25.8 kg m^{-3} potential density layer with anticyclonic subSIDDIES having their cores at 250-300 m along the 26-26.4 kg m^{-3} density layer. The SIDDIES corridor acts as a zonal pathway for both eddy-types to advect water masses and biogeochemical properties across the basin. This study provides a new insight on heat/salt fluxes, showing that 58% (32%) of the total heat eddy-flux is ascribed to cyclonic (anticyclonic) subSIDDIES, respectively, in the eastern South Indian Ocean. Anticyclonic subSIDDIES have also been found to be the sole high-saline water eddy-conveyor toward the western Indian Ocean.

1. Introduction

Mesoscale eddies are ubiquitous features of the world oceans and play a fundamental role in transferring physical and biological properties across different spatial and temporal scales (Chaigneau et al., 2011; Chelton et al., 2011; Dufois et al., 2017; Qiu & Chen, 2005; Zhang et al., 2014, 2015). The paradigm of a mesoscale eddy, known as a surface-intensified eddy, features the occurrence of maximum geostrophic velocities at the surface. Other types of eddies in the ocean which have their cores in the subsurface layer, are known as subsurface eddies or subsurface vortices (Kostianoy & Belkin, 1989; Mcwilliams, 1985). These can further be classified as subthermocline eddies (STEs), with the core below the thermocline, and intrathermocline eddies (ITEs), with the core between the seasonal and permanent thermoclines (Barceló-Llull et al., 2017; Li et al., 2017; Nauw et al., 2006; Pelland et al., 2013; Zhang et al., 2015). The focus of this particular study is on surface and subsurface eddies in the Southern Indian ocean without distinguishing between different subsurface eddy-types.

Surface signatures associated with subsurface eddies may be evident in some cases (Li et al., 2017). A peculiarity of subsurface cyclonic (anticyclonic) vortices is bowl (dome)-shaped isopleths in the shallower levels, and dome (bowl)-shaped isopleths in the deeper levels, with the cyclonic-associated shape termed as" thinny" by McGillicuddy (2015). These features trap vertically homogeneous water properties (McGillicuddy et al., 2007) from their area of origin. A key attribute of these eddies is that they are long-lived and hence,

trapped waters, representative of their formation area, are advected thousands of kilometers away (Nauw et al., 2006). This process could represent an important contribution to the oceanic heat and salt budgets as well as transport of biological tracers (Dong et al., 2014).

Subsurface eddies have been investigated in different parts of the global oceans, most extensively in the Pacific (Chaigneau et al., 2011; Collins et al., 2013; Li et al., 2017; Pelland et al., 2013; Thomsen et al., 2016; Zhang et al., 2015) and Atlantic (Barceló-Llull et al., 2017; Bower et al., 1997, 2013; McDowell & Rossby, 1978) Ocean compared to the Indian Ocean (Nauw et al., 2006; Shapiro &Meschanov, 1991). The most studied subsurface vortices are the deep, warm and salty Mediterranean water eddies (Meddies) (Bashmachnikov et al., 2015; Carton et al., 2010; Hebert et al., 1990; L'Hégaret et al., 2014) and the California Undercurrent eddies (Cuddies) (Collins et al., 2013; Garfield et al., 1999), both formed owing to baroclinic instabilities of their respective undercurrents namely the Mediterranean Undercurrent and the California Undercurrent. Another mechanism is the reduction of potential vorticity in frontal regions associated with opposite-directed winds on the frontal jet (Thomas, 2008). Three other mechanisms have been deduced from a numerical study of ITES in the Japan Sea (Hogan & Hurlburt, 2006): 1) subduction of winter surface mixed layer water at frontal convergence; 2) advection of stratified water capping a pre-existing eddy and; 3) a restratification of the upper layers in a pre-existing eddy due to solar heating. Lastly, McGillicuddy (2015) has recently proposed another generation mechanism where eddy-wind interactions drive a local upwelling so intense that it induces doming of isopycnals in anticyclonic eddies.

In the South Indian Ocean, two anticyclonic subsurface eddies, identified as ITEs, were surveyed southeast of Madagascar during the Dutch-South African ACSEX programme (Agulhas Current Sources EXperiment) (Nauw et al., 2006). Characterized by a subsurface maximum in salinity exceeding 35.8 psu, these flat, homogeneous water lenses had oxygen-rich cores. Nauw et al. (2006) tracked these anticyclonic eddies back to their generation area based on their water mass properties, namely, the Subtropical Underwater (STUW). High evaporation associated with low precipitation in the eastern South Indian Ocean induce an increase in sea surface salinity. The subsurface eddies appear in this high surface salinity region, which is also an important shear zone between the shallow eastward South Indian Ocean Countercurrent (SICC) (Jia et al., 2011a; Palastanga et al., 2007; Siedler et al., 2006) and the underlying westward South Equatorial Current. Owing to local instabilities between the currents, this highly saline water subducts in deeper layers, hence creating a subsurface salinity maximum. Interannual modulations of the eddy kinetic energy (EKE) in this zonal band (15°S-35°S) was shown to result from the variation of large-scale wind forcing by the Southern Annular Mode (Jia et al., 2011b). Anomalous gyre-scale upwelling or downwelling induces slackening or steepening of the isotherms and thus reduced or enhanced baroclinic instabilities and eddy activities, also at seasonal time scale (Jia et al., 2011b).

To the best of our knowledge, after the study of Nauw et al. (2006), which reported for the first time the presence of anticyclonic subsurface vortices in the South Indian Ocean, no other work has explored further the implications of these features to the Indian Ocean circulation. Some open questions remain: 1) What is the actual role of subsurface eddies within the context of heat and salt redistribution at mid-depths of the South Indian Ocean?; and 2) Do subsurface cyclonic eddies also exist in the South Indian Ocean? To answer these questions, we developed a subsurface eddy-identification method to distinguish between surface and subsurface eddies from a blended Argo-altimetry analysis. We present a three-dimensional eddy census and statistical characterization of surface and subsurface eddies in the South Indian Ocean along with the first climatological estimates of their associated volume, heat and salt transports.

This paper is structured as follows: The data sets, regions of study and subsurface eddy identification method are detailed in section 2. Section 3 deals with the results and discussion, with a description of surface and subsurface eddy demography and their mean (thermohaline and dynamic) vertical structures in section 3.1; the characteristics of the vertical structures of the subsurface eddies as well as their pathways in section 3.2; and their associated heat and freshwater fluxes in section 3.3. Section 4 summarizes the results.

2. Data and Methods

2.1. Eddy Available Potential Energy (EAPE)

The Eddy Available Potential Energy (EAPE) in the ocean is an energy budget, different from the kinetic energy reservoir, which indicates mesoscale turbulence at depth (Roullet et al., 2014). Analogous to active

baroclinic instabilities, this data set is based on ~830,000 Argo profiles spanning from 2002 to 2013. Anomalies in the vertical isopycnal displacement are used as a proxy to compute the intensity of the mesoscale subsurface turbulence. A practical method of computing EAPE is:

$$EAPE = -\frac{g}{2\rho_0}\overline{\zeta'\rho'} \quad (1)$$

where ζ' is the vertical isopycnal displacement, ρ' the density anomaly associated with this displacement, g is the gravitational acceleration (9.81 m s^{-2}), ρ_0 the potential density of seawater (1,024 kg m^{-3}) and the bar referring to a long-term time averaging. However, internal tides and waves, as well as the seasonal modulation in mixed layer can affect the signal. Consequently, it should be considered in regions remote to internal tides generation. From the maps shown by Arbic et al. (2012), we can infer that the eastern box is not influenced by internal tides. Although the western box is found on the southern boundary of internal tides hotspots (Mascarene Plateau), it is not greatly influenced by these features either. Further details on this product are provided by Roullet et al. (2014).

A peculiarity of the South Indian Ocean is its level of eddy energy in its eastern basin (Jia et al., 2011a), as is apparent in Figure 1a. An enhanced EAPE signature, as well as EKE, are evident in both the eastern and western boundary current systems, namely the Leeuwin Current and the South East Madagascar Current. It should be noted that the EAPE is shown in Figure 1b at 150 m depth, where Nauw et al. (2006) observed the eddy core of subsurface eddies. The boxes outlined in Figures 1a and 1b indicate the two study regions: an" eddy generation region" (eastern box at 85°E to 110°E) proposed by Nauw et al. (2006), and an" eddy arrival region" (western box at 50°E to 75°E), where 2 subsurface eddies have been previously observed (Nauw et al., 2006), both at a latitude range of 20°S-32°S.

The eastern box encloses the region where subsurface eddies have been shown to be generated via subduction of high saline water. This eddy generation site is collocated with the enhanced signal of EAPE near 100°E, shown within the box in Figure 1b. The western box was based on the observations reported by Ponsoni et al. (2015, 2016), which suggest that altimeter-detected eddies drive a significant variability of the

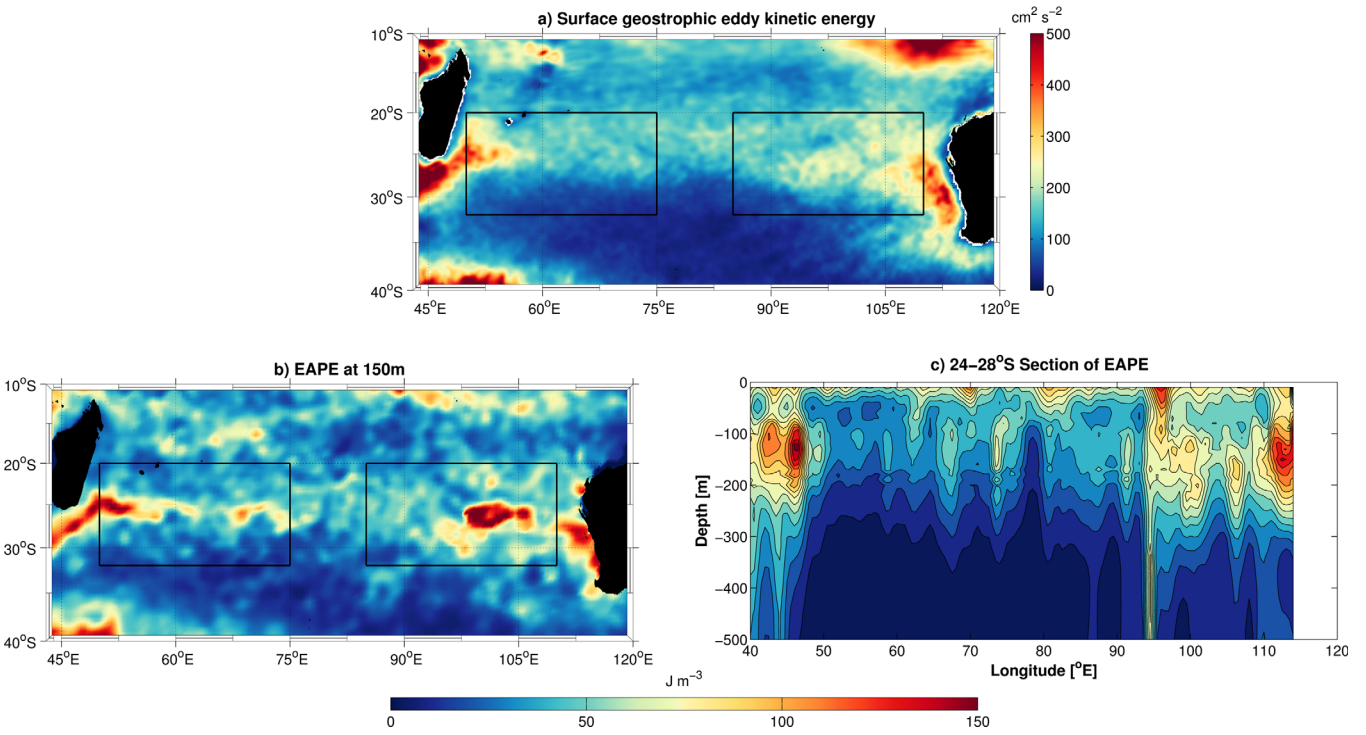

Figure 1. (a) Mean surface geostrophic eddy kinetic energy (EKE; cm^2 s^{-2}) calculated from 12 years (2002–2013) AVISO data. **(b)** Mean EAPE (J m^{-3}) at 150 m depth with two black boxes delineating regions of interest. **(c)** shows a mean latitudinal (24°S-28°S) vertical section of EAPE across the South Indian Ocean (40°E to 120°E).

volume transport carried by the EMC. In accordance with these findings, the western box was located in the open ocean, before interaction with the EMC, so that the properties of the eddies are captured prior to their arrival to the western boundary. This western box forms part of an" eddy-corridor" described by Quartly et al. (2006), and which has been associated with the westward-propagating mesoscale eddies. These two distinct zones are separated by the low subsurface EAPE signature observed at approximately 78°E (Figure 1b) and are located well into the open ocean.

2.2. Eddy Tracking Algorithm

In this study, the 4^{th} release of an existing eddy global data set (Chelton et al., 2011) was used to identify and study mesoscale eddies in the South Indian Ocean. This data set is established from an automated algorithm which tracks eddies based on daily sea surface height (SSH), as seen from altimetry in the delayed-time" two-sat merged" product of AVISO. Computed relative to a 20-year altimeter reference period, this altimeter product was gridded at daily intervals on a 0.25° x 0.25° Cartesian grid.

The eddy data set version used here takes a simple approach based on Williams et al. (2011), by locating pixels with maximum/minimum SSH and finding the neighbouring pixels of SSH values with decreasing/increasing thresholds, using a threshold increment of 0.25 cm from −100 cm to +100 cm (Schlax & Chelton, 2016). Five well-defined criteria based on the number of pixels forming an eddy, *E*, are used to mark the end of its life. *E* must be connected by a maximum of 2,000 pixels, with a minimum of 2 interior pixels and no" holes" in the eddy. No pixel in *E* can have a neighbouring pixel of another eddy, and the maximum distance over all pairs of edge pixels in *E* must be less than 400 km. See Schlax and Chelton (2016) for a detailed description of approach and criteria.

This data set provides the amplitude, radius, propagation speed, vorticity as well as the start and end locations of the eddy life. All eddies tracked for less than 4 consecutive weeks were removed from the data set so as to lessen the probability of false eddies that may come up from SSH fields' noise. This 4-week lifetime was chosen as it corresponds to the 35-day e-folding time scale of the Gaussian covariance function, during the objective analysis procedure which is used to construct SLA fields of AVISO Reference Series (Chelton et al., 2011).

The eddies in the two regions of study were selected based on two different criteria. In the eastern box, mesoscale eddies with their genesis occurring within the box were taken into consideration. In the western box, all eddies passing through it were considered, either locally or remotely generated.

2.3. Argo Float Data

Initially designed for large-scale climate studies (Riser et al., 2016), the international Argo program, which consists of almost 3,800 autonomous Lagrangian profiling floats in January 2018, has recently been used to study oceanic mesoscale eddies in different parts of the world oceans (Chaigneau et al., 2011; Li et al., 2017; Yang et al., 2015; Zhang et al., 2014). These floats provide freely available temperature and salinity data from the surface to as deep as 2,000 m (Coriolis Project: http://coriolis.eu.org). For the three-dimensional study of surface and subsurface eddies propagating in the South Indian Ocean basin, we use profiles from August 2000 to December 2015. These data have undergone automatic pre-processing and quality control measures by the Argo Data Centre (Böhme & Send, 2005; Owens & Wong, 2009; Wong et al., 2003). To ensure that only good data was retained, the following two criteria, based on the quality control flags and sampling characteristics of the Argo data, were used: (1) Only temperature, salinity and pressure data with quality flag 1 (good) and 2 (potentially good) were considered; (2) It was ensured that each profile contained a shallow data point between 20 m depth and the surface, as well as a deep data point below 1,500 m, to maximise the number of profiles suitable for our study. A common depth at 1,500 m was chosen as a reference level to compute the steric dynamic height anomalies used in the eddy identification algorithm (Yang et al., 2015). Near the surface, only profiles which sampled the first 20 m of the water column were considered to ensure that shallow eddy signatures are capture when present. A survey of automated visual inspection ensured the goodness of the identification algorithm performance and any suspicious profiles were discarded.

The above criteria were applied after an eddy-Argo collocating analysis was performed. Assuming a perfect circular eddy-shape, all Argo profiles located within the eddy-radius distance from the eddy-core are taken into consideration. At this stage, Argo profiles are also identified as either anticyclonic or cyclonic,

depending on the eddy altimeter database. In the eastern Indian Ocean region, this technique provided 1,232 and 1,191 profiles in anticyclonic (AEs) and cyclonic eddies (CEs) respectively, whereas in the western region, it yielded 1,232 profiles in AEs and 1,451 profiles in CEs. The combined 5,106 T/S profiles were interpolated on a regular 10 m vertical grid from the surface down to depth. The temperature, salinity and potential density anomalies of each profile associated with the two eddy categories (AE and CE) were then calculated by removing the climatological values from the CSIRO Atlas of Regional Seas 2009 (CARS09) data set (Dunn & Ridgway, 2002; Ridgway et al., 2002), which have been spatially and temporally interpolated to match the exact day in year and positions of the profiles. This enabled the quantification of the eddy properties different to the background field and, therefore their potential role in the redistribution of heat and salt in the ocean.

2.4. Subsurface Eddy Identification Method

The combination of the Argo and eddy-database led to 5,106 Argo profiles co-located to altimeter-detected eddies. However, among these Argo profiles, one may find the signal of either surface or subsurface eddies; the latter type only when they also have a surface signature. The challenge is to set an automated algorithm which will assign the above number of Argo profiles to surface or subsurface eddies. To this aim, first we compute their steric dynamic change. The variability in steric change is due to changes in either the subsurface temperature profiles (thermosteric component) and/or in the subsurface salinity profiles (halosteric component). For each profile, the *Steric Dynamic Height Anomaly (SDHA)*, h', was computed using a reference level at 1,500 dbar, following the definition by Gill and Niiler (1973) and Tomczak and Godfrey (1994):

$$h' = \int_{-1500}^{0} \delta\rho \; dz \tag{2}$$

where $\delta\rho$ is the density anomaly of the profile, relative to CARS09, and dz is the vertical grid resolution. 1,500 dbar has been commonly referenced as no-motion in former studies in this region (Yang et al., 2015). For any co-located Argo-eddy profile, a dynamic height anomaly more significant in the subsurface compared to the surface layers, would be representative of subsurface maximum in velocities associated with the eddy, hence a subsurface-intensified eddy. It should be noted that steric height anomalies may represent the signature of internal tides. The implication of internal tides on the two boxes of interests have been discussed in section 2.1.

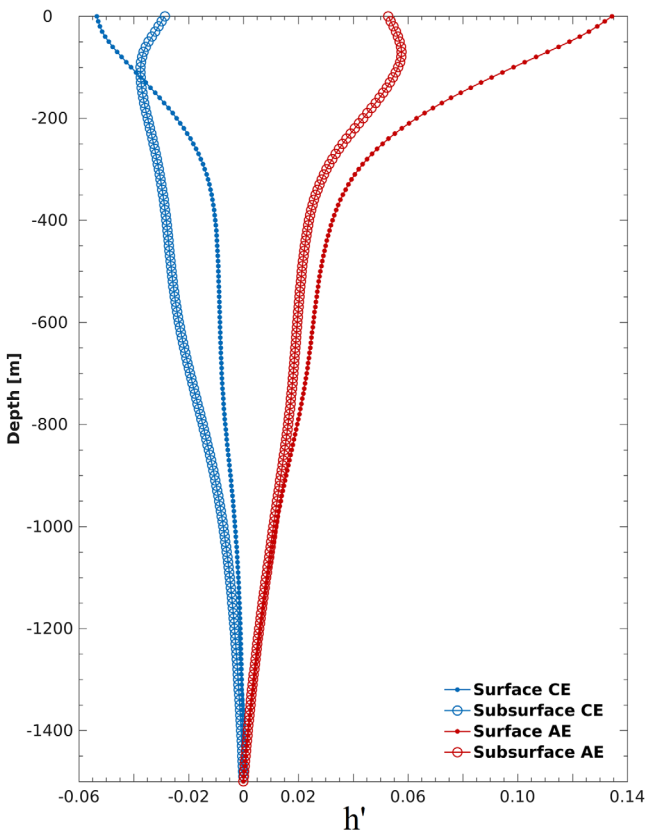

Figure 2. Steric Dynamic Height anomaly, h', (m) for surface (small dots) and subsurface (large dots) intensified cyclonic (blue) and anticyclonic (red) eddies

Applying this specific criterion to identify subsurface eddies, 474 CEs and 135 AEs profiles in the eastern South Indian Ocean, and 368 CEs and 168 AEs in the western part were characterized as subsurface-intensified. Figure 2 illustrates the difference in steric dynamic height anomalies of surface and subsurface eddies in the South Indian Ocean. Cyclonic profiles characterized as subsurface cyclonic eddies displayed more negative steric dynamic anomalies in their subsurface layers. For subsurface anticyclonic eddies, the profiles exhibited more positive anomalies of steric dynamic height in their subsurface levels. On the other hand, surface-intensified profiles are very distinct with large anomalies at the surface, representative of maximum velocities at the surface. However, it is worthwhile recalling that in Figure 2, only subsurface eddies with a surface signature are included since they were altimeter-detected. Concurrently, submesoscale eddies account for 54% of the total number of eddies in the South Indian Ocean (Zheng et al., 2015) and are not considered here, given the spatial resolution of the altimeter product. These imply an underestimation of the total number of surface and subsurface eddies.

It is worthwhile noting that the accuracy of this method relies on the characteristic vertical distance between surface and subsurface anomalies of steric dynamic height. A high vertical resolution of

temperature and salinity is required such that the characteristic difference between SDHAs is well solved. In this study, the mean vertical sampling resolution of Argo floats in the eastern and western Indian Ocean was 8.7 ± 1.4 m and 8.4 ± 1.6 m, respectively; whereas mean vertical distances between surface and subsurface peaks in SHDA were 80 (110) m for AEs (CEs). Based on the latter, one can reasonably argue that we are well above the requirement to solve indistinctly the difference between surface and subsurface eddies. The applicability of this eddy identification method to other regions of the global oceans will depend on the above discussed relationship between vertical scales of surface against subsurface eddies and vertical sampling rates of temperature and salinity data.

2.5. Eddy Composition

To reconstruct the 3-dimensional structure (temperature, salinity and potential density) of each eddy-type, we assume a rotationally symmetric eddy with cylindrical shape. The zonal and meridional distances (Δx and Δy respectively) are defined relative to the eddy centre, where $\Delta X = \Delta Y = 0$. For the eddy composites, a normalized coordinate system is used, where the distance of each Argo profile to the eddy centre, denoted as 'r', is normalized by the eddy radius, R.

For each level of depth (z), the variables and their respective anomalies are transformed onto a normalized horizontal eddy-coordinate system (ΔX, ΔY). These are then mapped onto a regular 0.5° X 0.5° grid using the Barnes objective analysis (Barnes, 1973). This method consists of an inversed distance weighting interpolation and has previously been used in mesoscale eddy structures studies (Yang et al., 2013, 2015). The variables are then extracted in 1-D as a function of the distance r/R to the eddy centre. A regression fitting curve, LOESS (Locally Weighted Scatter-plot Smoother) (Cleveland & Devlin, 1988) is then applied to the 1-D data set at each level z to prevent the presence of any discontinuity in the composites. Eventually, all the variables, v (r,z), are mirrored to v (-r,z) for graphics.

From the composite vertical potential density, $\bar{\rho}$ (r, z), the composite vertical rotational speed ($\bar{v}$) is calculated using the thermal wind balance equation:

$$\bar{v}(r,z) = -\frac{g}{f}\int_{-1500}^{z}\frac{\partial \rho\,(r,z)}{\partial r}\,dz \tag{3}$$

where f is the mean Coriolis parameter (-0.64 x 10^{-4} s^{-1}) over the latitudinal band.

3. Results and Discussions

3.1. Eddy Statistics and Vertical Structures

In this section, we present the statistics and typical three-dimensional structures of the four eddy-types (cyclonic/anticyclonic and surface/subsurface), for both the eastern and western South Indian Ocean regions.

3.1.1. South Eastern Indian Ocean

The mean statistical characteristics of the different eddy types generated in the eastern South Indian Ocean region are displayed in Table 1. Surface AEs have been more often detected than surface CEs, and this is consistent with a higher occurrence of AEs in the Eastern South Indian Ocean (Zheng et al., 2015). The number of Argo profiles tracked in surface eddies is also greater than for subsurface eddies, as one might expect. The weaker, and sometimes even absent surface signal of subsurface eddies enables the collocation of a lower number of Argo profiles as compared to the number of Argo profiles in surface eddies: 43% (11%) of the total of profiles corresponded to cyclonic (anticyclonic) subsurface eddies. In this context, we do not have enough information to argue that the lower percentage of subsurface AE profiles compared to CE profiles respond to either an actual lower percentage of subsurface AEs or to a lower retention capacity of the subsurface AEs. Remarkably, subsurface eddies outlive surface eddies, with a mean lifespan of approximately 217 (CEs) and 223 days (AEs) compared to 175 (CEs) and 185 (AEs) days for surface eddies. This supports the suggestion of the important role of subsurface eddies for the re-distribution of ocean properties as their natural tendency to propagate westward from the east will take them toward the western margins of the basin.

No major differences are observed between the rotational and translational speeds of the different eddy-types. They present similar mean radius ranging from 100–115 km, consistent with Dufois et al. (2014), who

Table 1
Statistical Characteristics of Surface and Subsurface Eddies in the Eastern South Indian Ocean

	Surface		Subsurface	
Eastern Indian Ocean	CE	AE	CE	AE
Number of profiles	779	1190	605	151
Lifespan (days)	185 ± 169	175 ± 158	217 ± 189	223 ± 168
Amplitude (cm)	9.0 ± 4.7	9.6 ± 4.7	10.0 ± 5.9	7.6 ± 4.1
Radius (km)	115.3 ± 36.3	115.8 ± 32.1	103.9 ± 39	111.7 ± 31.1
Rotational speed (cm s^{-1})	25.0 ± 8.9	25.6 ± 7.6	26.8 ± 9.6	22.3 ± 7.0
Translational speed (cm^{-1})	4.5 ± 1.7	4.7 ± 1.9	4.6 ± 1.7	4.5 ± 1.4

Nore. ± refers to the standard deviation from the mean.

also showed averaged eddy radius of the order of 100 km in the South Indian Ocean. The amplitude reveals no great variation among the different eddy-types. However, the mean amplitude for cyclonic vortices are higher compared to anticyclonic ones. This is in agreement with Chelton et al. (2011) who showed larger amplitude associated with CEs in the Southern Hemisphere, a feature linked to a rotational speed greater than 20 cm s^{-1}.

Figure 3 shows temperature and salinity anomalies of the four distinct eddy-types in a cross section passing through the centre of the composite eddies. Note that the two subsurface AEs surveyed by Nauw et al. (2006) in 2001 near Madagascar, whose origin were suggested to be in the eastern Indian Ocean, were characterized by subsurface positive salinity anomalies in their cores. In agreement with Nauw et al. (2006), the subsurface eddy-identification method used here reveals a positive salinity anomaly in the subsurface levels of these eddies (see Figure 3d for CEs and Figure 3h for AEs). These vertical salinity structures give us confidence in our subsurface-eddy identification method.

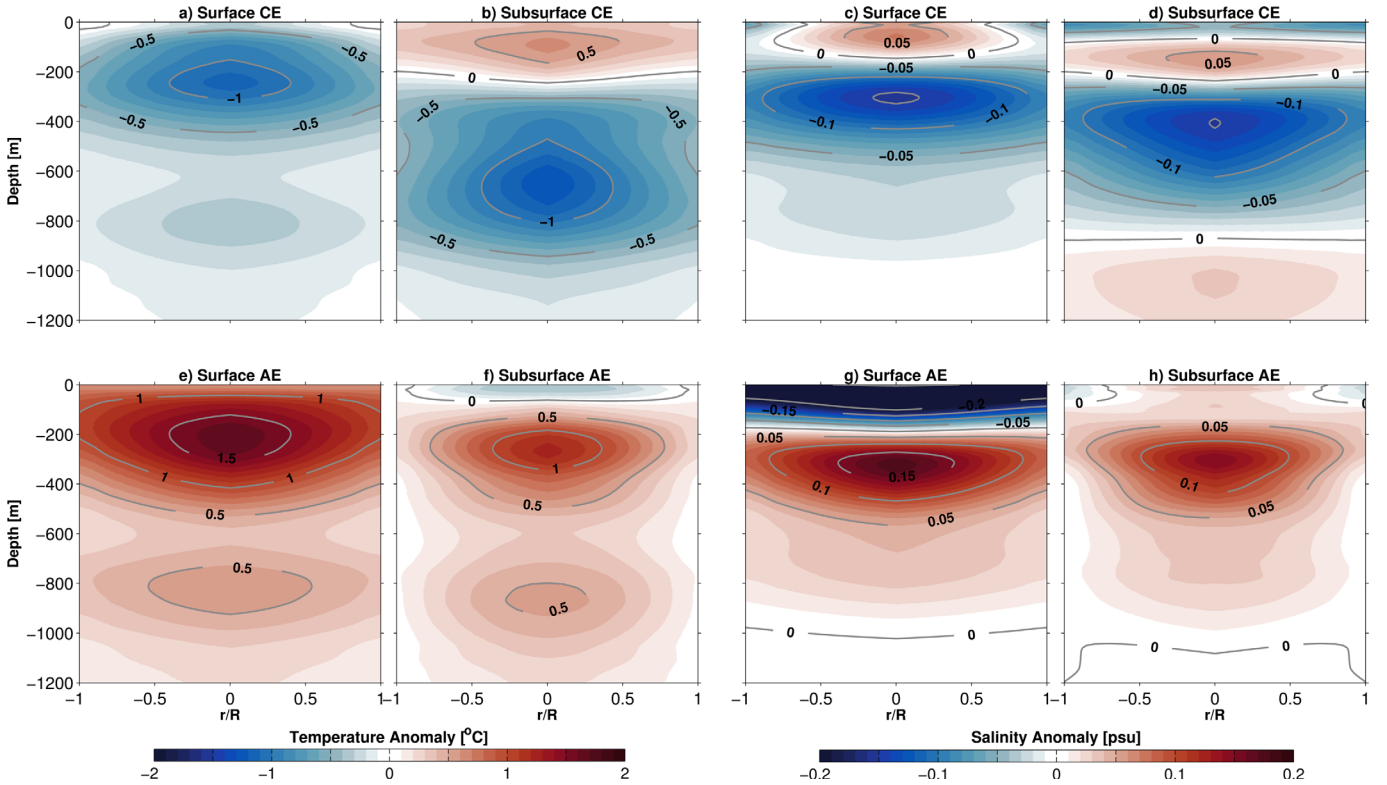

Figure 3. Vertical sections of potential temperature (°C; 1st and 2nd columns; a,b,e,f) and salinity anomalies (psu; 3rd and 4th columns; c,d,g,h) across composite cyclonic (top) and anticyclonic (bottom) surface and subsurface eddies, at $\Delta Y = 0$, in the eastern South Indian Ocean, over the box shown in Figure 1a.

We find that the composite vertical structures of surface and subsurface eddies, after performance of the automated identification algorithm, agree well with expectation according to their associated vertical displacements. Thus, composite eddies present a positive salinity maximum at subsurface levels when vertical movement subducts surface high salinity water at depth. This occurs in both surface and subsurface AEs (Figures 3g and 3h). Interestingly, surface AEs differ in the upper layers from subsurface AEs with a salinity minimum, absent in the latter (Figure 3h). Also as expected in subsurface CEs, a positive subsurface salinity maximum occurs at ∼150 m depth, with significant negative anomalies in the deeper layers (∼400 m; Figure 3d). Castelao (2014) showed that positive but small surface salinity anomalies are associated with CEs, owing to their vertical displacements. This is in agreement with the slightly positive surface salinity anomaly present in surface CEs Figure 3c).

The eddy-vertical temperature structures also follow expectations from their associated vertical displacements, with both surface and subsurface CEs (AEs) being responsible in moving colder (warmer) waters. In both surface CEs and AEs, the same polarity in temperature anomalies prevail throughout the structure, with negative and positive anomalies respectively (Figures 3a and 3e). However, subsurface eddies reveal two cores of temperature anomalies, of different polarities. Subsurface CEs display positive anomalies in their surface and negative anomalies in their subsurface layers. The contrary occur in subsurface AEs, with negative and positive anomalies in their surface and subsurface layers, respectively. The negative core of subsurface CEs is located at around ∼650 m, deeper than subsurface AEs positive core which is found at ∼300 m. Another interesting note is the occurrence of a clear, near-zero temperature anomaly which coincides with the depth of the STUW in the South Indian Ocean, at ∼200 m depth (O'Connor et al., 2005) (see section 3.2).

The mean vertical structure of rotational speed associated with each different eddy-type in the eastern South Indian Ocean is calculated using the thermal wind balance (Equation 3), and is shown in Figure 4. As expected, maximum rotational speeds prevail in the deeper levels for subsurface CEs and AEs (Figures 4b and 4d), compared to surface CEs and AEs which exhibit maximum speed at the surface (Figures 4a and 4c).

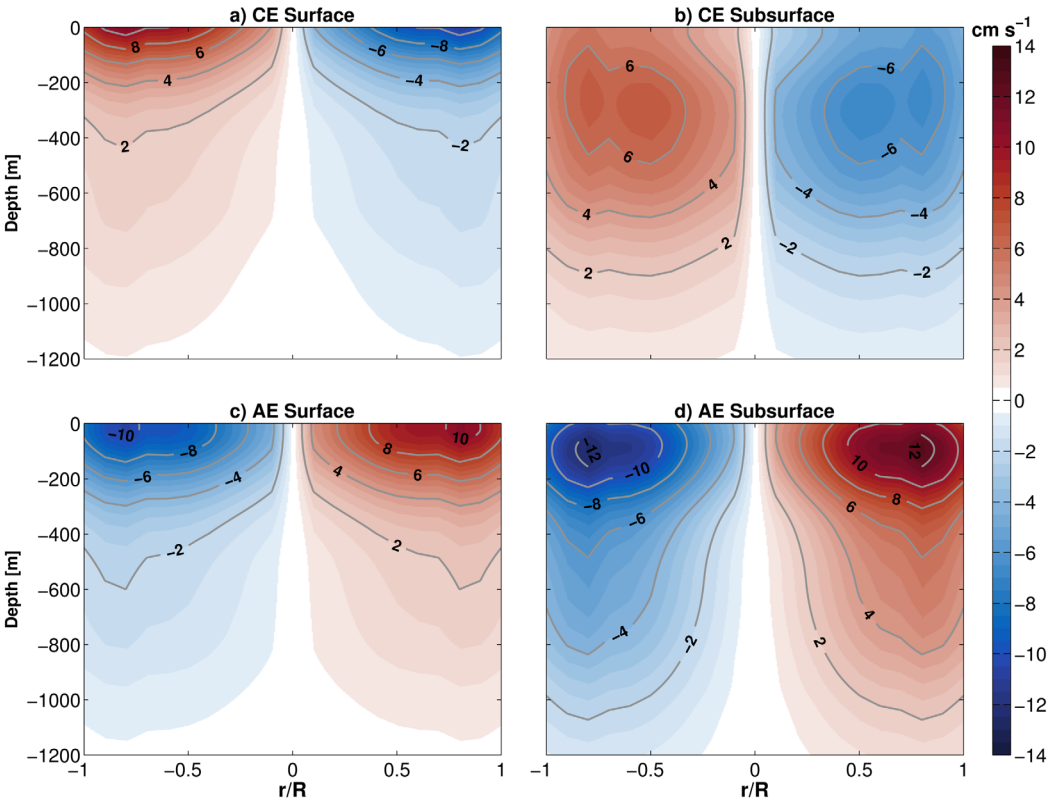

Figure 4. Vertical sections of the rotational speed anomaly (cm s^{-1}) of the composite surface CEs (a) and AEs (c) and subsurface CEs (b) and AEs (d) in the eastern Indian Ocean.

Rotational speeds of subsurface AEs are generally stronger than subsurface CEs, but with the vertical extent of enhanced speed being smaller and shallower. Note that the former exhibits almost two times the rotational speed of subsurface CEs. Maximum magnitudes of 12.6 cm s^{-1} and 6.8 cm s^{-1} occur at ~100 m and ~300 m depth for subsurface AEs and CEs respectively, compared to a surface magnitude of 10–11 cm s^{-1} for surface AEs and CEs. The rotational speed of surface eddies extends down to ~1,000 m, compared to subsurface eddies which influence deeper levels, sometimes down to 1,200 m, as suggested by Nauw et al. (2006)who surveyed two subsurface AEs with vertical structures down to ~1,000 m.

3.1.2. South Western Indian Ocean

Statistical characteristics of the different eddy-types in the western South Indian Ocean are displayed in Table 2. Compared to the eastern box, more (less) subsurface AEs (CEs) are tracked in the western box, accounting to a total of 14.9% (28.8%) of all western AEs (CEs) profiles. As observed in the eastern South Indian Ocean, these subsurface features are longer-lived compared to surface ones. Considering the altimetric expression of the different eddy-types, no significant differences are observed. However, the mean translational speeds in the western box exceed those in the eastern box by almost 0.75 cm s^{-1}.

Generally, the thermohaline vertical structures of the distinct eddy-types in the western South Indian Ocean Figure 5) are analogous to the eastern region (generation site; Figure 3), with similar vertical structures but at weakened intensities. Subsurface eddies are characterized by positive salinity anomalies, with surface AEs differentiating from subsurface AEs with a negative surface salinity anomaly. Owing to their associated upwelling (downwelling) mechanisms, as expected, CEs (AEs) display negative (positive) temperature anomalies. However, as observed in the eastern region, their subsurface forms exhibit two cores of opposite polarities. Their respective surface signature is characterized by a negative sign of the surface paradigm, and only the subsurface water column is consistent with the expected uplift/downlift of isotherms. This interesting feature of opposite vertical temperature polarities associated with subsurface eddies needs to be taken into consideration when investigating the biogeochemical implications associated with surface and subsurface eddies in the South Indian Ocean.

The magnitude of the rotational speed associated with surface eddies in the western South Indian Ocean (Figure 6). remain quite coherent, when compared to the eastern box (Figure 4). On the other hand, subsurface eddies, especially CEs, decrease in strength. They exhibit maximum magnitudes of 3 cm s^{-1} and 11 cm s^{-1} for subsurface CEs and AEs respectively. However, subsurface CEs have maximum speeds closer to the surface, compared to the maximum being at ~50 m depth for AEs. This maximum is closer to the eddy-center, in relative to the subsurface AEs in the eastern box. This may be due to the long-lived dynamics of subsurface eddies, which lose their rotational speeds' intensity far from their generation site. Collectively with shorter lifetimes and comparable rotational speeds, this supports the idea that most surface eddies are originated either locally or in adjacent areas.

A band of high eddy kinetic energy (EKE) occurs at 25°S in the South Indian Ocean, linking the eastern to the western basin (Jia et al., 2011a). Along this band, mesoscale eddies, which we suggest to be referred to as 'SIDDIES' (South Indian ocean eDDIES), propagate westward toward Madagascar. Apart from their cyclonic and anticyclonic vorticity contrast, we have shown that SIDDIES can occur as two distinct features; namely, surface-intensified and subsurface-intensified SIDDIES. Adding to the" eddy-zoo", we suggest that these two eddy-types be referred as" surfSIDDIES" and" subSIDDIES" respectively.

Table 2
Statistical Characteristics of Surface and subsurface Eddies in the Western South Indian Ocean

	Surface		Subsurface	
Western Indian Ocean	CE	AE	CE	AE
Number of profiles	1158	1304	469	229
Lifespan (days)	161 ± 123	150 ± 113	171 ± 128	158 ± 124
Amplitude (cm)	8.8 ± 4.7	9.3 ± 4.5	8.2 ± 4.3	7.8 ± 4.0
Radius (km)	116.0 ± 33.1	119.8 ± 33	118.4 ± 34.0	115.4 ± 31.4
Rotational speed (cm s^{-1})	23.5 ± 8.9	23.8 ± 7.5	22.2 ± 8.3	21.2 ± 6.7
Translational speed (cm^{-1})	5.3 ± 2.6	5.4 ± 2.7	5.4 ± 2.5	5.3 ± 2.3

Note. ± refers to the standard deviation from the mean.

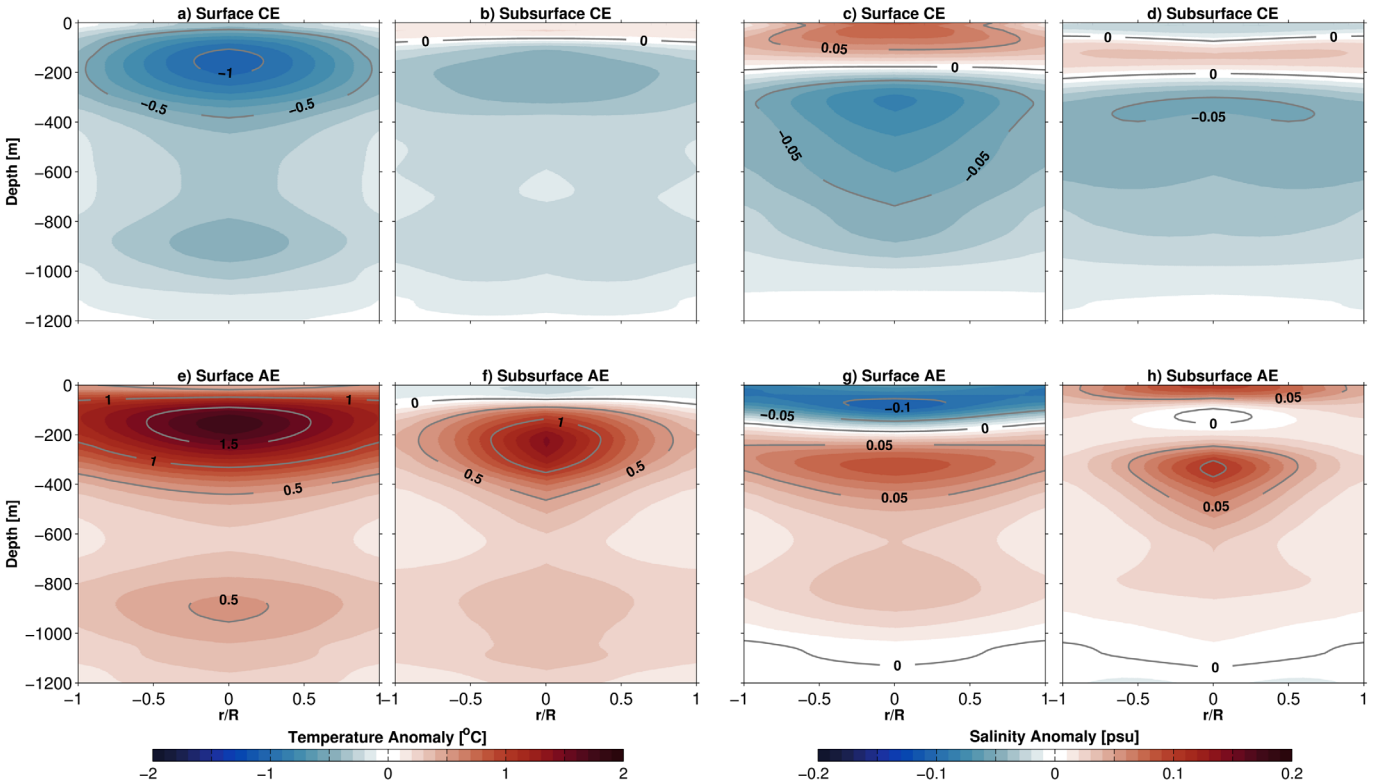

Figure 5. Vertical sections of potential temperature (°C; 1st and 2nd columns) and salinity anomalies (psu; 3rd and 4th columns) across composite cyclonic (top) and anticyclonic (bottom) surface and subsurface eddies in the western Indian Ocean.

SubSIDDIES were characterized by subsurface salinity maximum signatures, with their mean cores at ∼150–200 m in cyclonic (Figures 3d and 5d) and ∼250–300 m in anticyclonic forms (Figures 3h and 5h). A recent subsurface anticyclonic eddy surveyed south of the Canary Islands in the North Atlantic Ocean (Barceló-Llull et al., 2017), as well as anticyclonic eddies in the South Pacific Ocean (Chaigneau et al., 2011) have quite similar vertical haline structure as anticyclonic subSIDDIES. Characterized by warm-water lens in subsurface layers, they exhibit a small cap of cold water at the surface, consistent with Barceló-Llull et al. (2017), where they suggest it to be due to the seasonal thermocline shoaling. Hence, the key attributes of anticyclonic subSIDDIES are a slight (significant) positive salinity anomaly at the surface (subsurface) levels, accompanied by a negative (positive) temperature anomalies at the surface (subsurface) levels.This structure is in agreement with the PUMP eddy structure (Barceló-Llull et al., 2017). Although less observed in open ocean, cyclonic forms of subsurface eddies do occur in the South Indian Ocean. However, compared to anticyclonic subSIDDIES, their positive subsurface salinity signature is weaker. These eddies, travelling in a preferential latitudinal band, form an eddy corridor between the eastern and western South Indian Ocean, as we will see in the following section.

3.2. SubSIDDIES Vertical Characteristics and Propagation

This section investigates subSIDDIES vertical characteristics and how these features propagate westward from the eastern South Indian Ocean basin. Based on Nauw et al. (2006) as well as on Figures 3 and 5, the depth at which maximum positive salinity anomalies prevail, for Argo profiles falling within the subsurface vortices category are considered. We will refer to this as the 'maximum salinity depth'. In both the eastern and western South Indian Ocean, the preferential maximum salinity depth lie between 75 and 150 m with ∼42% (∼60%) of AEs (CEs) being in this depth range. Subsurface AEs have a secondary deeper preferential maximum salinity depth with almost 30% lying between 200–300 m and 250–350 m in both the eastern and western South Indian Ocean respectively (Figures 7a and 7c). This is in agreement with upwelling/downwelling which will push (drag) the maximum salinity depth to shallower (deeper) levels. For cyclonic subSIDDIES, we find that preferential salinity depths do not vary significantly between both study regions.

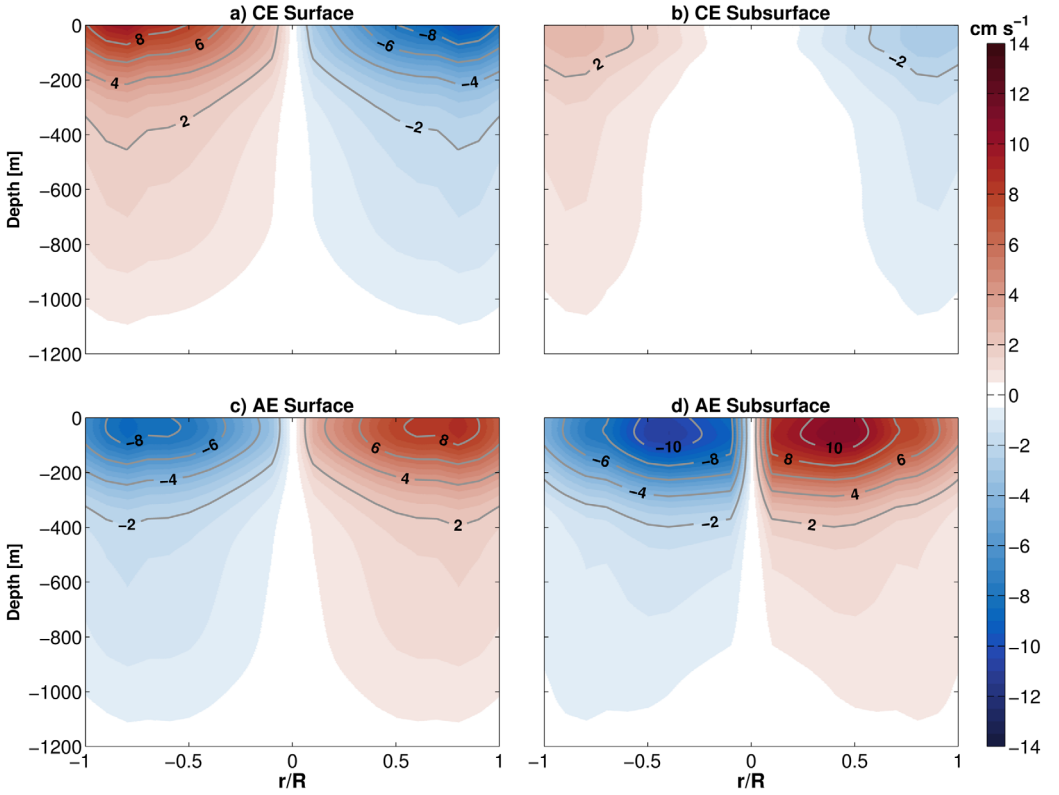

Figure 6. Vertical sections of the rotational speed anomaly (cm s^{-1}) of the composite surface CEs (a) and AEs (c) and subsurface CEs (b) and AEs (d) in the western Indian Ocean.

Potential densities corresponding to the maximum salinity depth in the eastern region range from 26-26.8 kg m^{-3} for AEs and 25.8–26.2 kg m^{-3} for CEs (Figure 7b), with 44% (33%) of subsurface AEs (CEs) being in the 26.2–26.6 (26-26.4) kg m^{-3} range. The associated upper and lower bounds are within the domain of the highly saline STUW (Hanawa & Talley, 2001; O'Connor et al., 2005). In the western region, the potential density in cyclonic subSIDDIES is more spread from 25.4–26 kg m^{-3}, with another peak between 26.6–26.8 kg m^{-3} (Figure 7d). However, 60% of AEs potential density ranges from 25.8 to 26.4 kg $^{-3}$. Generated in a region of water mass formation (eastern box), eddies would trap waters with distinct water mass properties. However, AEs appear to be more coherent while propagating westward, retaining greatly their original water mass properties (Figures 7b and 7d). Observed differences might be the response to diffusion processes, interannual variations in the θ/S properties of the water masses of origin as proposed by Nauw et al. (2006) or because of eddies surveyed in the western box being generated far from the eastern box

Following the assumption that subsurface lenses migrate along isopycnal surfaces and consequently conserve their water mass properties during this propagation (Mcwilliams, 1985), the pathways linking the western to the eastern South Indian Ocean is backtracked in Figure 8. Subsurface CEs and AEs in the western South Indian Ocean have potential density ranges of 25.4–25.8 kg m^{-3} and 26-26.4 kg m^{-3}, accounting for 23% and 46% respectively. These preferred density ranges for cyclonic (anticyclonic) subSIDDIES are consistent with the density ranges of Peru-Chile Current System (PCCS) eddies where CE (AE) cores correspond to 25.2–26 (26-26.8) kg m^{-3} (Chaigneau et al., 2011). The low percentage of CEs in the given density range might be attributed to the spread of the eddy core over a wider potential density range (Figure 7d).

Figure 8a reveals the favoured CE isopycnal layers which links the eastern to the western South Indian Ocean at 200 m, 150 m and 100 m depth, accounting for 75% of CEs having their maximum salinity depth within that range. On the other hand, denser water present in the AE deeper layers links the two regions at 250 m, 200 m and 150 m depth. 37% of AEs have their maximum salinity within these depths, with 38% being at shallower depths. This variability can possibly be explained through the seasonal modulation of the depth of isopycnal layers in the region.

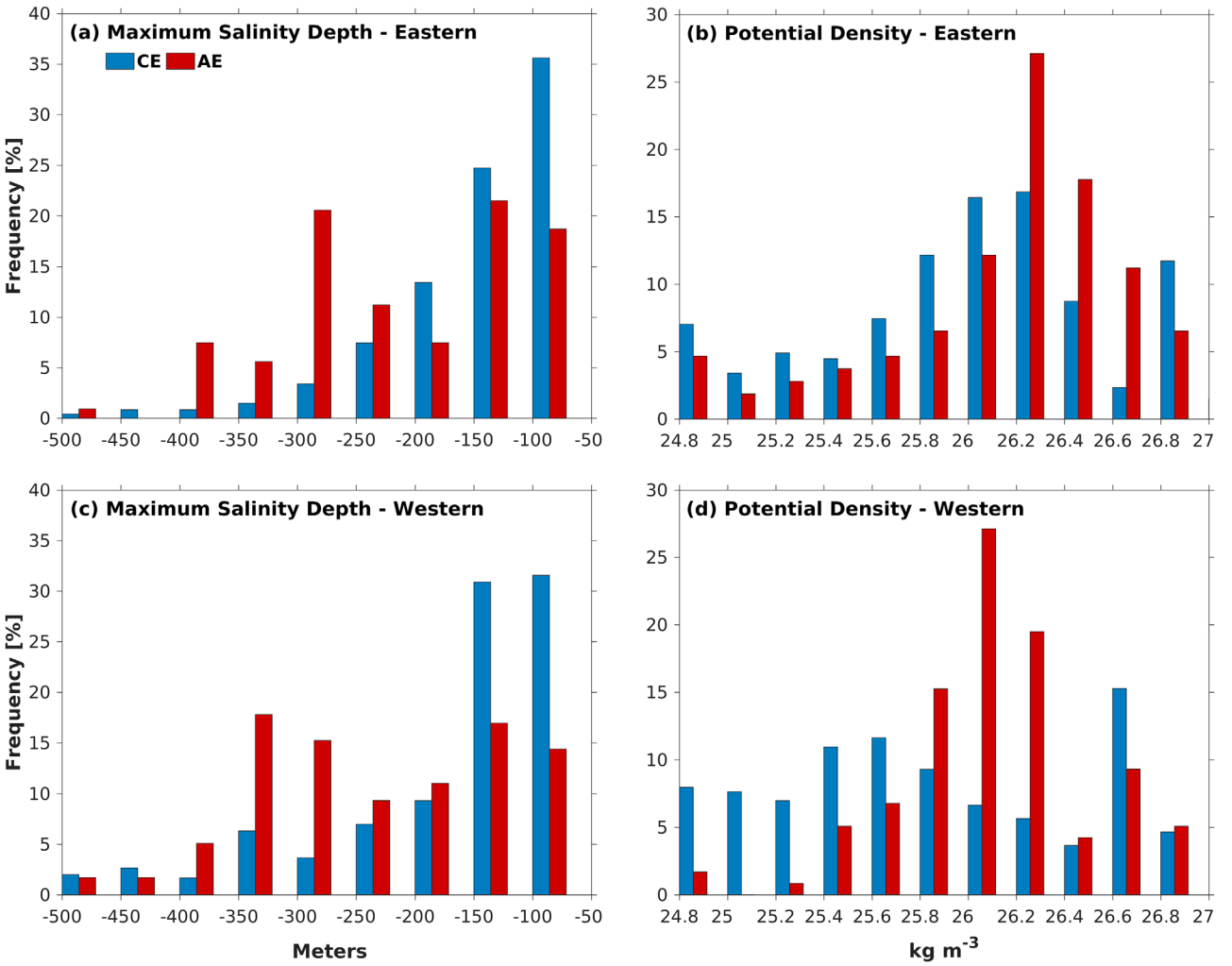

Figure 7. Histogram distribution of maximum positive salinity depths and their corresponding potential density of subSIDDES in the eastern Indian Ocean (a, b) and western Indian Ocean (c, d).

These pathways are further confirmed when investigating the generation sites as well as the trajectories of the subSIDDIES in the eastern (Figures 8c and 8d) and western (Figures 8e and 8f) South Indian Ocean. One important note is that these are only eddies with surface signatures and which have been surveyed at least once by an Argo profile, hence leading to an underestimation of the subsurface eddy tracks. The equatorward (poleward) tendencies of subsurface AEs (CEs) are due to their propagation on a β-plane, and the meridional drift of the eddies which is induced by the change in relative and planetary vorticities on their flanks (Morrow et al., 2004).

Surface as well as subsurface eddies connect the eastern to the western South Indian Ocean basins, along isopycnal layers. These pathways, corroborated by the eddy tracks in Figures 8c–8f, are suggestive of a continuous eddy corridor between Australia and Madagascar, coinciding with the high zonal EKE band at 25°S (Figure 1a) where large eddies ($R > 100$ km) are observed, as shown by Zheng et al. (2015). We can conclude that this is a preferential latitudinal band of propagation for SIDDIES and, therefore, we suggest to name this latitudinal band in the South Indian Ocean as the 'Corridor of SIDDIES', analogous to the Canary Eddy Corridor (Sangrà et al., 2009). This corridor suggests a possible key role of these features (surfSIDDIES and subSIDDIES) in the redistribution of warm and fresh water, as well as other variables such as nutrients and trace elements.

3.3. Heat and Freshwater Fluxes

The ocean's role in the global heat balance is fundamental due to its ability to transport excess heat from the tropics toward the poles. The oceanic circulation is responsible for most of this poleward heat transport,

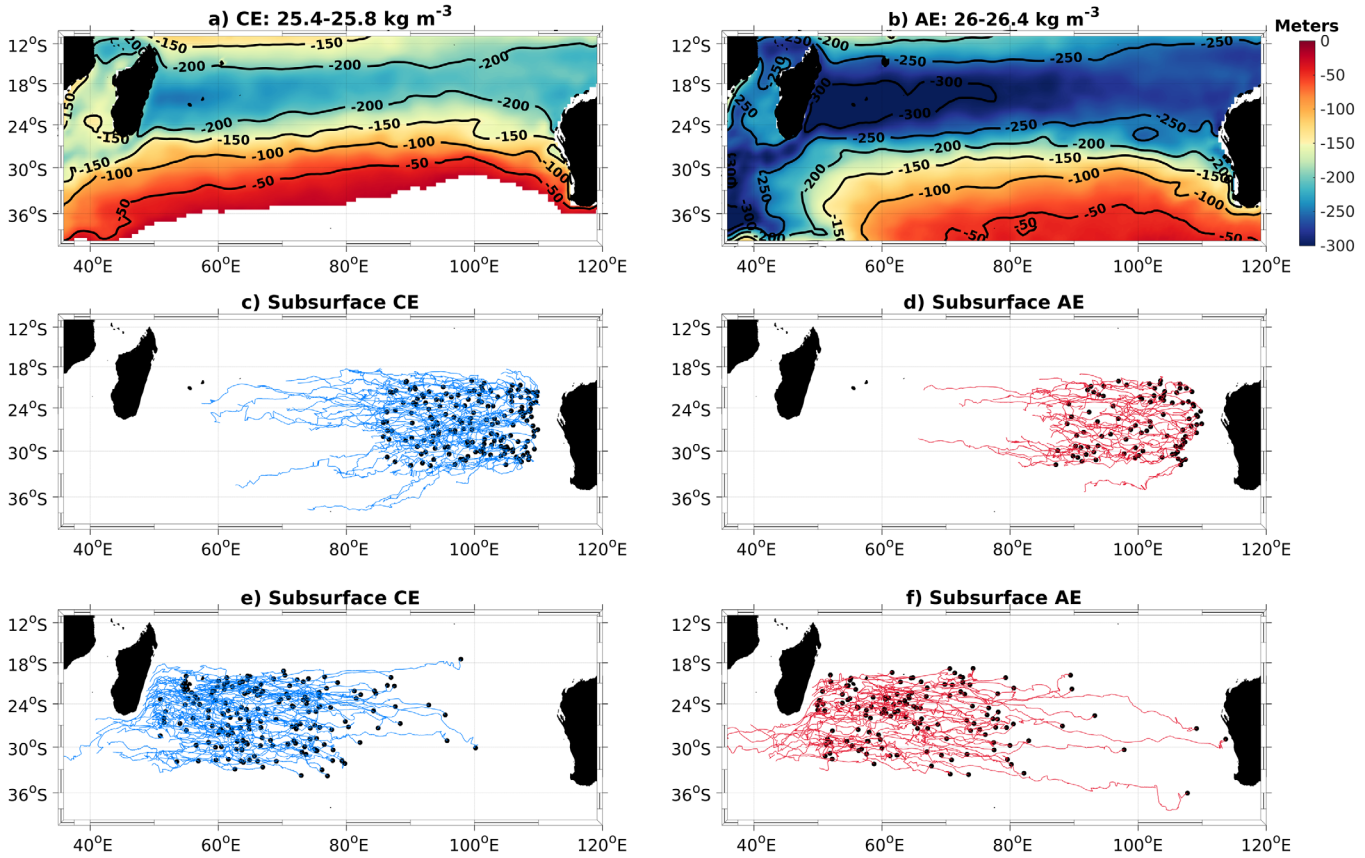

Figure 8. First row displays depth of isopycnal layers corresponding to favoured water mass properties of (a) cyclonic and (b) anticyclonic subSIDDIES. Second and third rows show the tracks of subSIDDIES studied in the eastern (c and d) and western (e and f) South Indian Ocean, with blue (red) indicating CE (AE).

partly through mesoscale eddies (Dong et al., 2014; Robinson, 1983; Volkov et al., 2008). This section estimates the heat and freshwater fluxes associated with the four eddy-types of study. Flierl (1981) suggested that the volume of trapped water in an eddy is dependent on the ratio of its rotational and translational speeds, also known as the nonlinearity parameter, with a ratio exceeding 1 implying a coherent eddy structure during its propagation (Chelton et al., 2007, 2011). Accordingly, we compute the mean vertical structures of nonlinearity for cyclonic/anticyclonic surfSIDDIES/subSIDDIES in both western (Figure 9a) and eastern (Figure 9b) regions.

In the eastern South Indian Ocean, the deep vertical stretch of cyclonic and anticyclonic subSIDDIES associated with the existence of subsurface eddy-cores results in a large vertical area of trapped fluid, down to 630 m and 780 m respectively, compared to their analogous surface eddies with trapped fluid extending down to 190 m and 260 m respectively. Generally speaking, the extent of trapped water in the western side of the basin is much lower, with a depth of 250 m for anticyclonic subSIDDIES, and 160 m (190 m) for cyclonic (anticyclonic) surfSIDDIES. However, the non-linearity parameter associated with cyclonic subSIDDIES reveals no trapped fluid, owing to their low rotational speed, as seen in Figure 6b. It must be noted that we are underestimating the rotational speed in our case, since only the geostrophic and not the ageostrophic component of the eddy is taken into consideration. Penven et al. (2014) and Barceló-Llull et al. (2017)showed that the ageostrophic part could contribute to 30–40% of the geostrophic component of anticyclonic eddies. Only absolute in-situ measurements of this eddy-type will help to better elucidate its non-linearity parameter.

Overall, this results in a more significant volume advected through subsurface eddies compared to surface features, and hence will have a greater impact on the warm and fresh water distribution in the South Indian Ocean. The available heat and salt content anomalies (AHA and ASA respectively) of the four eddy-types are computed, as in Chaigneau et al. (2011), to estimate how much warm and fresh water is being transported.

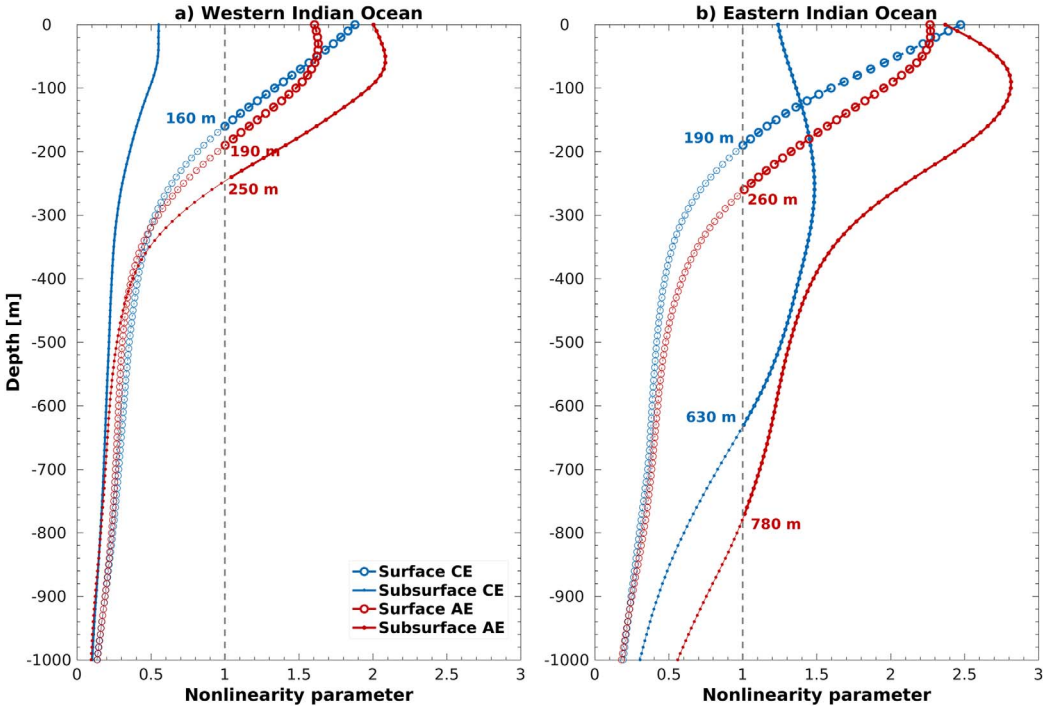

Figure 9. Mean vertical profiles of the nonlinearity parameter of the four eddy-types (surface and subsurface CEs and AEs) for the western (a) and eastern (b) South Indian Ocean.

The AHA and ASA are derived from the following equations:

$$AHA = \int_{Ztrap}^{0} \int_{0}^{Rc} \rho_0 \; Cp \; \theta' \, (2\pi r) \, dr \; dz \tag{4}$$

$$ASA = 0.001 \int_{Ztrap}^{0} \int_{0}^{Rc} \rho_0 \; S' \, (2\pi r) \, dr \; dz \tag{5}$$

where C_p is the specific heat capacity (4,000 J kg $^{-1}$ K $^{-1}$) and R_c the mean eddy radius. The temperature and salinity anomalies (θ' and S′ respectively) are integrated over the eddy-core area by assuming a circular symmetrical shape, and then vertically integrated over the trapping depth (Z_{trap}). We also integrate radially from the eddy centre to the eddy-core radius, with R_c being the mean eddy radius of the four distinct eddy-types. A 0.001 factor is used for ASA so as to convert salinity to salinity fraction (kg of salt per kg of seawater).

Focusing on the" eddy-generation region" namely the eastern South Indian Ocean, the vertical profile of AHA (Figure 10a) reveals a more significant negative (positive) anomalies associated with cyclonic (anticyclonic) surfSIDDIEs compared to their subSIDDIES counterpart. However, when integrating from the surface to the trapping depths, cyclonic subSIDDIES advect larger AHA values (-5.1 x 10^{18} J) compared to surfSIDDIES one (-3.8 x 10^{18} J) (Table 3). Furthermore, anticyclonic surfSIDDIES carry slightly larger AHA (10.8 x 10^{18} J) compared to their subSIDDIES counterpart (9.4 x 10^{18} J). In contrast to subsurface vortices in other regions, cyclonic subSIDDIES exhibit almost similar heat anomalies (-5.1 x 10^{18} J) to PCCS eddies (-5.5 x 10^{18} J) (*Chaigneau et al.*, 2011), whereas anticyclonic subSIDDIES display higher available heat content than the PUMP eddy (2.9 x 10^{18} J) (Barceló-Llull et al., 2017), Cuddies (0.36 x 10^{18} J) (Pelland et al., 2013) and PCCS eddies (8.7 x 10^{18}J) (Chaigneau et al., 2011). This difference in heat content can be dependent on the radius of the eddy, which is larger for subSIDDIES (∼115 km) compared to PUMP (∼30 km), Cuddies (∼20 km) and PCCS eddies (∼60 km), as well as the much deeper associated trapping depths.

For the available salt content anomalies, subSIDDIES play a more influential role on the total salt redistribution in the South Indian Ocean, primarily due to their positive/negative salt content (Figures 10b and 10d) and larger vertical extent of trapped volume (Figure 9). Anticyclonic surfSIDDIES show salt deficiencies

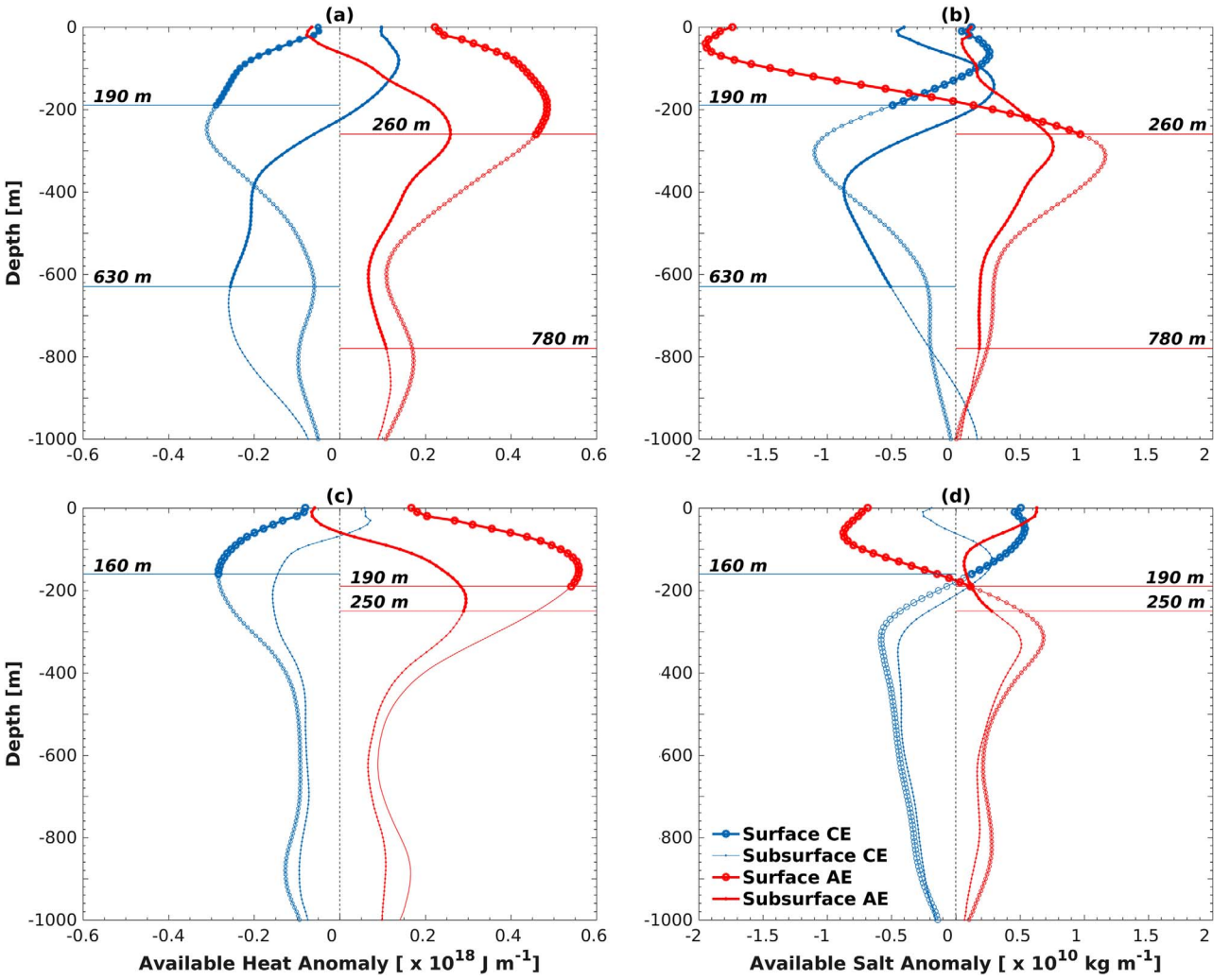

Figure 10. Mean available heat anomaly (J m^{-1}; left column) and available salt anomaly (Kg m^{-1}; right column) associated with the four eddy-types in the eastern (first row) and western (second row) South Indian Ocean.

Table 3
Vertical Extent, Volume, Thermohaline Contents and Associated Heat/Freshwater Flux of Four Distinct Eddy-Types in the Western and Eastern Indian Ocean Regions

	Western Indian Ocean				Eastern Indian Ocean			
	Surface		Subsurface		Surface		Subsurface	
	CE	AE	CE	AE	CE	AE	CE	AE
Vertical Extent [m]	0 - 160	0 - 190	-	0 - 250	0 - 190	0 - 260	0 - 630	0 - 780
Volume [x 10^{12} m^3]	6.8	8.6	-	10.5	7.9	11	21.4	30.6
AHA [x 10^{18} J]	−3.3	8.4	-	3.8	−3.8	10.8	−5.1	9.4
Zonal Q_{eh} [TW]	−0.62	1.7	-	0.4	−0.6	1.7	−0.6	0.8
Meridional Q_{eh} [TW]	−0.06	−0.02	-	−0.04	0.04	0.12	0.04	0.07
ASA [x 10^{10} Kg]	6.7	−10.8	-	6.1	0.6	−19.8	−25.6	27
Zonal Q_{fw} [Sv]	−0.4	0.6	-	−0.2	−0.02	0.9	0.8	−0.7
Meridional Q_{fw} [Sv]	−0.03	−0.007	-	0.02	0.002	0.06	−0.05	−0.06

(−19.8 x 10^{10} Kg) with respect to the background water mass, whereas subSIDDIES transport a surplus of saline water (27 x 10^{10} Kg). Anticyclonic subSIDDIES, compared to other eddy-types in the region, transport large salt content anomalies (27 x 10^{10} Kg), which is of the same order of salt content of AEs in PCCS (23.8 x 10^{10} Kg) (Chaigneau et al., 2011). Moreover, cyclonic surfSIDDIES carry a slight excess salt (0.6 x 10^{10} Kg) with cyclonic subSIDDIES being deficient in salt (−25.6 x 10^{10} Kg) (Table 3).

In the western Indian Ocean, cyclonic subSIDDIES do not seem to play a significant role in the heat and freshwater advection owing to their weak rotational speed, with no apparent capacity to transport water (Figure 9a). The other eddy-types show similar AHA and ASA vertical structures to the eastern region but with shallower trapping depths. As seen in sections 3.1 and 3.2, SIDDIES lose their characteristics partially during the westward migration and this could explain the lower integrated AHA and ASA. Anticyclonic surfSIDDIES are again shown to correspond to freshwater content whereas both cyclonic surfSIDDIES and anticyclonic subSIDDIES have positive salt content anomalies.

SIDDIES have the ability to advect mass, heat and freshwater in distinct depth layers, depending on the ratio between their rotational and translational speeds. Hence, their respective zonal heat and salt transports (Zonal Q_{eh} and Zonal Q_{es}) as well as their meridional components (Meridional Q_{eh} and Meridional Q_{es}) for each eddy-type are computed for the eastern and western South Indian Ocean boxes (Table 3). We do this through longitudinal (97.5°E for eastern and 62.5°E for western region) and latitudinal (26°S) sections centered on the 2 boxes. The associated total time-mean fluxes are estimated by multiplying the average eddy properties by their respective population density number, N_e, where N_e is the total number of each eddy-type passing through the longitudinal and latitudinal sections divided by their corresponding time length, as in Duncombe Rae et al. (1996) and Chaigneau et al. (2011). Salt transport is interpreted as freshwater flux (unit: Sv), with $Q_{fw} = - Q_{es}/\rho_0 S_o$, where $S_o = 35$ psu (salt mass fraction) is the mean upper ocean salinity. It should also be noted here that the associated eddy-fluxes are from the surface down to the specific trapping depth of each eddy-type.

The resultant fluxes associated with each eddy-type as well as the net eddy fluxes are also displayed in Figure 11. The mass flux of all eddy types is representative of their westward displacement, with slightly

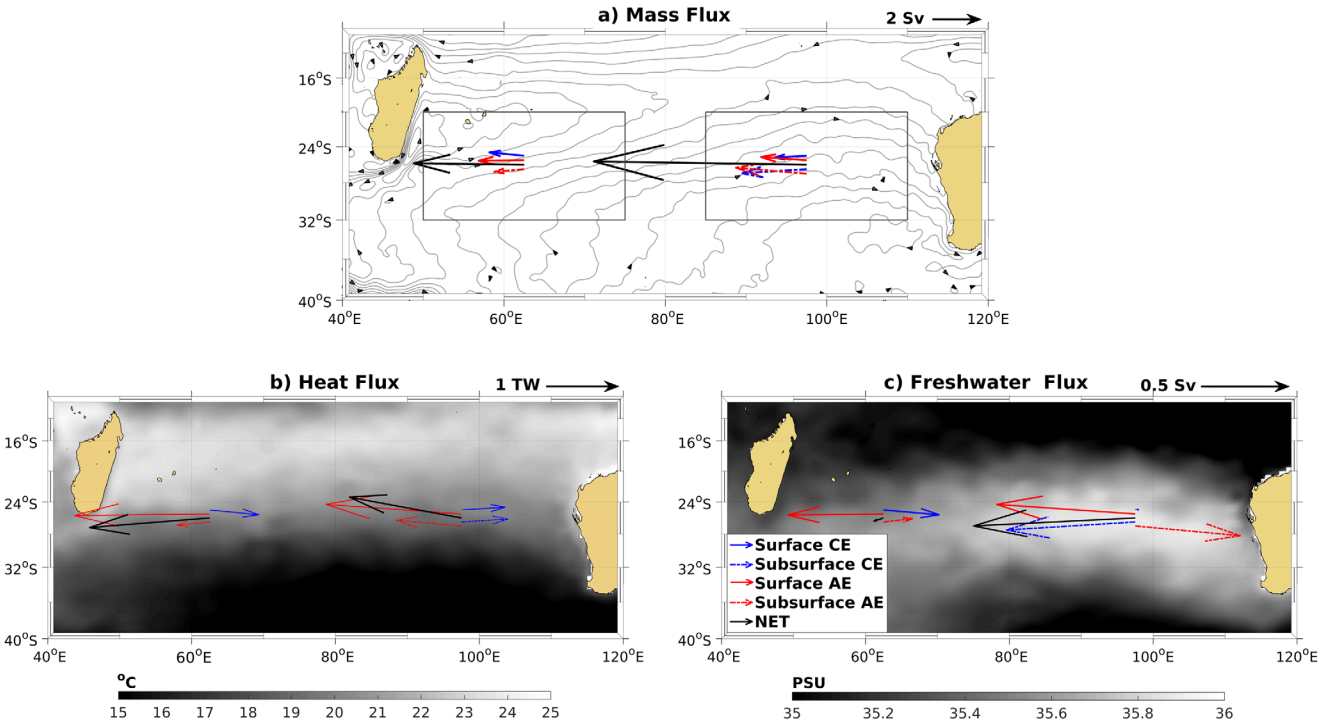

Figure 11. Resultant vectors associated with the mass (a), heat (b) and freshwater flux (c) of each eddy-types (see legend), in the eastern and western South Indian Ocean region. The background displays (a) streamlines of sea surface height representing geostrophic mean circulation, (b) salinity and (c) temperature, both salinity and temperature averaged between 50 and 150m depth.

equatorward (poleward) deflections for anticyclonic (cyclonic) surfSIDDIES and subSIDDIES in the eastern South Indian Ocean, as expected. This westward migration of the cyclonic and anticyclonic eddies induce a zonal heat transport, that tend to offset each other to some extent, due to their opposite signs. Meridional heat transport, however, will combine to give larger values. Comparatively with freshwater fluxes, this is not always the case.

Consistent in terms of direction, the net-eddy heat flux is, however, of a lesser magnitude compared to Volkov et al. (2008) and Dong et al. (2014), owing to a basin-wide context in their studies. In the eastern region, anticyclonic subSIDDIES advect 50% less heat (0.81 TW) compared to anticyclonic surfSIDDIES (1.7 TW). This is due to the colder water in the surface layers of anticyclonic subSIDDIES compared to the warmer water for surfSIDDIES. However, cyclonic surfSIDDIES (0.6 TW) and subSIDDIES (0.6 TW) display quite similar heat transport. Anticyclonic (cyclonic) surfSIDDIES advect 6 (3) times more heat compared to PCCS anticyclonic (cyclonic) eddies which advect 0.28 (-0.17) TW. A net equatorward heat flux toward a temperature upgradient is observed in the eastern Indian Ocean (Figure 11b), owing to a preferential equatorward movement of anticyclonic vortices (and poleward movement of CEs) (Chelton et al., 2007; Morrow et al., 2004), and their associated large vertical trapping depths (Figure 9b). SubSIDDIES have a net eddy-heat flux of ∼3% of the total global northward heat component (∼50–60 TW), between the latitudinal band of 20°S-32°S (Dong et al., 2014; Jayne & Marotzke, 2002). Taking into account the underestimation of the number of subsurface eddies in our study due to only altimeter-detected eddies being considered, associated heat-flux could be an important integral of the global net eddy-heat flux.

In the western Indian Ocean, we observe the same phenomenon with AEs, with their surface form moving warmer water (1.7 TW) compared to their subsurface form (0.41 TW). The net eddy heat flux of 1.5 TW is slightly poleward. This can be attributed to the presence of the shallow SICC (Palastanga et al., 2007; Siedler et al., 2006) which flows against the mean eddy propagation (Figure 11a), as well as the sub-gyre east of Madagascar, which can interact with the mesoscale eddies and their poleward/equatorward affinities. The 1.5 TW eddy-heat flux could contribute to the 100 TW conveyed by the Agulhas Current (Volkov et al., 2008) and the 62 TW transported by the Agulhas rings (Souza et al., 2011) into the South Atlantic Ocean. This inter-ocean exchange of heat and salt, on longer timescales, could alter the variability Meridional Overturning Circulation (Beal et al., 2011; Biastoch et al., 2008).

An interesting feature of the South Indian Ocean is the presence of a high subsurface salinity in the eastern basin. One might expect that mesoscale eddies formed in this region would advect this high saline water westward. However, a westward freshwater flux through eddies is predominant. This flux is associated with all eddy-types, except anticyclonic subSIDDIES (Table 3), and is largely controlled by the extent of their trapping depths. A shallow trapping depth of 260 m for anticyclonic surfSIDDIES infer fresher surface water advection compared to the deeper saltier water (Figure 3g).

With positive salt content anomalies along their trapping depths, anticyclonic subSIDDIES are found to be the sole saline-water (23.3×10^3 Kg s^{-1}) eddy-conveyor toward the western region, in their subsurface layers. This is consistent with the two anticyclonic subSIDDIES surveyed close to Madagascar in 2001 (*Nauw et al*., 2006). Cyclonic surfSIDDIES exhibit positive as well as negative salt content anomalies in their trapping depth, resulting in a small eastward freshwater flux. The net eddy-freshwater flux is westward, south-westward at a magnitude of ∼0.98 Sv.

The westward freshwater flux associated with anticyclonic surfSIDDIES in the western box is compensated by the eastward salt flux exhibited by cyclonic surfSIDDIES and anticyclonic subSIDDIES. The net eddy freshwater flux is however westward slightly poleward in the western South Indian Ocean regions (Figure 11c). The western South Indian Ocean region, being the" eddy-arrival region", is expected to reveal different fluxes compared to the eastern part. This may be due to different factors namely: 1) more coherent structures of mesoscale eddies in the east generate more significant fluxes; 2) freshwater input from the Indonesian Throughflow into the eastern region significantly influences the salt advection; 3) the presence of the SICC and the sub-gyre south-east of Madagascar can interact and influence incoming eddies and/or shed its own eddies; and finally 4) the loss, to some extent, of the eddy properties during their long-lasting life.

Dong et al. (2014) reported a freshwater flux of −0.1 Sv to −0.2 Sv, at latitudes 20°S and 32° respectively, with a positive freshwater flux (0.1 Sv) observed at ∼25°S. The net eddy-freshwater flux in the eastern region (0.98 SV) accounts for almost 10 times more than reported (Dong et al., 2014). A more important

number of subSIDDIES would imply a greater impact of freshwater flux on the main oceanic currents in the vicinity, and eventually on the Agulhas Current System. It is important to note that some uncertainties are associated with the fluxes. These are because only surface-detected eddies are taken into consideration, the computation of rotational speed is based on a level of no-motion which is not always the same in different part of the global ocean, and the ageostrophic component of the eddy is not being accounted for. Hence, in the western basin, cyclonic subSIDDIES could still advect water even when our current results suggest otherwise. From these, stronger fluxes than stated here could be inferred.

4. Summary and Future Work

The South Indian Ocean is characterized by a zonal band of high EKE, the only one occurring at a subtropical eastern boundary of the global oceans (Jia et al., 2011a). Among other features, we attribute this enhanced EKE to westward-propagating South Indian Ocean eddies, which we termed in this study as 'SIDDIES'. SIDDIES can occur in two forms namely surface-intensified or subsurface-intensified. On the basis of an eddy tracking scheme (Chelton et al., 2011) and available Argo profiles, we have devised a novel subsurface eddy identification method, based on their steric dynamic height anomalies. The eddy-subsurface identification method was successful in distinguishing between Argo profiles collocated in surface eddies and subsurface eddies. Hence, we propose that surface-intensified and subsurface-intensified eddies to be referred as" surfSIDDIES" and" subSIDDIES".

This study has characterized, for the first time, a mean vertical thermohaline structure of cyclonic and anticyclonic surface and subsurface eddies in the eastern (genesis area) and western South Indian Ocean, where only two subsurface AEs have been previously surveyed. This allows us to investigate their ability to transport properties to remote regions. SurfSIDDIES and subSIDDIES migrate from the eastern to the western South Indian Ocean, along preferential isopycnal layers. Cyclonic (anticyclonic) subSIDDIES, with their mean cores lying at ∼150–200 (250–300) m, prefer density layers of 25.4–24.8 (26-26.4) kg m^{-3}. We termed the preferential latitudinal band (15°S-35°S) the" SIDDIES Corridor". SubSIDDIES are found to contribute largely to the distribution of heat and salt in the South Indian Ocean. 58% (32%) of the total eddy-heat flux is attributed to cyclonic (anticyclonic) subSIDDIES in the eastern Indian Ocean whereas 58% is attributed to the total in the western region. In terms of fresher water, anticyclonic subSIDDIES account for 42.5% (24%) of the total freshwater fluxes in the eastern (western) regions, but in the opposite direction.

The results in this study highlight the importance as well as the contribution of subsurface-intensified eddies in the redistribution of heat and fresh water in the South Indian Ocean, and hence suggest that they might have an important role in the regional western boundary current system namely the Greater Agulhas Current System. The interesting dipole temperature structure associated with these subSIDDIES are worthy of further investigation due to its possible importance on the spatial distribution of SST and eventually on sea surface wind. The influence of eddies on the distribution of chemical tracers through horizontal and vertical advection have also been previously reported (Chelton et al., 2011; Gaube et al., 2013, 2014; Iskandar et al., 2010; McGillicuddy & Robinson, 1997). Thomsen et al. (2016) showed that subsurface anticyclonic eddies stir local tracers and then advect biological properties such as oxygen and nitrate from the PCCS slope toward the offshore open ocean where an oxygen minimum zone is present. This mechanism has also been documented in the South Indian Ocean which is known as a unique environment where chlorophyll-a concentration is maximum in anticyclonic eddies (Dufois et al., 2016, 2017). However, these studies deal with the mesoscale eddies as being surface-intensified eddies. Hence it will be important to the biogeochemical community to investigate how these special eddies, with their cores in the subsurface, transport nutrients or biomass through their long-lived journeys across the South Indian Ocean basin, and how they interact with the presence of the deep chlorophyll-maximum.

Acknowledgments
The eddy-tracking data set used in this study was developed by Dudley Chelton and Michael Schlax, and is available on the AVISO website as 'Mesoscale Eddy Trajectory Atlas' product. All the Argo profiles used in this study are freely available from the ARGO program website (http://doi.org/10.17882/42182; http://argo.ucsd.edu/). The authors are grateful to the two anonymous reviewers, whose constructive comments greatly improved this manuscript. Dilmahamod A.F. is supported by the National Research Foundation (NRF), South African Environmental Observation Network (SAEON), the International Centre for Education, Marine and Atmospheric Sciences over Africa (LMI ICEMASA) and the Institut de Recherche pour le Dveloppement (IRD).

References

Argo (2000). Argo float data and metadata from Global Data Assembly Centre (Argo GDAC). SEANOE. http://doi.org/10.17882/42182

Arbic, B., Richman, J., Shriver, J., Timko, P., Metzger, J., & Wallcraft, A. (2012). Global modeling of internal tides within an eddying ocean general circulation model. *Oceanography*, *25*(2), 20–29. https://doi.org/10.5670/oceanog.2012.38

Barceló-Llull, B., Sangrà, P., Pallàs-Sanz, E., Barton, E. D., Estrada-Allis, S. N., Martínez-Marrero, A., Aguiar-González, B., Grisolía, D., Gordo, C., Rodríguez-Santana, Á., Marrero-Díaz, Á., & Arístegui, J. (2017). Anatomy of a subtropical intrathermocline eddy. *Deep Sea Res. Part I Oceanogr. Res. Pap*, *124*, (April), 126–139. https://doi.org/10.1016/j.dsr.2017.03.012

Barnes, S. L. (1973). *Mesoscale objective map analysis using weighted time-series observations* (NOAA Tech Memo, ERL NSSL-62, 60 pp). Norman, OK: National Severe Laboratory,

Bashmachnikov, I., Neves, F., Calheiros, T., & Carton, X. (2015). Properties and pathways of Mediterranean water eddies in the Atlantic. *Prog.ress inOceanography*, *137*, 149–172. https://doi.org/10.1016/j.pocean.2015.06.001

Beal, L. M., De Ruijter, W. P. M., Biastoch, A., & Zahn, R. (2011). On the role of the Agulhas system in ocean circulation and climate. *Nature*, *472*(7344), 429–436. https://doi.org/10.1038/nature09983

Biastoch, A., Böning, C. W., & Lutjeharms, J. R. E. (2008). Agulhas leakage dynamics affects decadal variability in Atlantic overturning circulation. *Nature*, *456*(7221), 489–492. https://doi.org/10.1038/nature07426

Böhme, L., & Send, U. (2005). Objective analyses of hydrographic data for referencing profiling float salinities in highly variable environments. *Deep Sea Research Part II*, *52*(3–4), 651–664. https://doi.org/10.1016/j.dsr2.2004.12.014

Bower, A. S., Armi, L., & Ambar, I. (1997). Lagrangian Observations of Meddy Formation during A Mediterranean Undercurrent Seeding Experiment*. *Journal of Physical Oceanography*, *27*(12), 2545–2575. https://doi.org/10.1175/1520-0485(1997)027¡2545:LOOMFD>2.0.CO;2

Bower, A. S., Hendry, R. M., Amrhein, D. E., & Lilly, J. M. (2013). Direct observations of formation and propagation of subpolar eddies into the Subtropical North Atlantic. *Deep Sea Research Part II*, *85*, 15–41. https://doi.org/10.1016/j.dsr2.2012.07.029

Carton, X., Daniault, N., Alves, J., Cherubin, L., & Ambar, I. (2010). Meddy dynamics and interaction with neighboring eddies southwest of Portugal: Observations and modeling. *Journal of Geophysical Research*, *115*, C06017. https://doi.org/10.1029/2009JC005646

Castelao, R. M. (2014). Mesoscale eddies in the South Atlantic Bight and the Gulf Stream Recirculation region: Vertical structure. *Journal of Geophysical Research. Ocean*, *119*, 2048–2065. https://doi.org/10.1002/2014JC009796

Chaigneau, A., Le Texier, M., Eldin, G., Grados, C., & Pizarro, O. (2011). Vertical structure of mesoscale eddies in the eastern South Pacific Ocean: A composite analysis from altimetry and Argo profiling floats. *J. Journal of Geophysical Research*, *116*, C11025. https://doi.org/10.1029/2011JC007134

Chelton, D. B., Schlax, M. G., & Samelson, R. M. (2011). Global observations of nonlinear mesoscale eddies. *Progress in Oceanography*, *91*(2), 167–216. https://doi.org/10.1016/j.pocean.2011.01.002

Chelton, D. B., Schlax, M. G., Samelson, R. M., & de Szoeke, R. A. (2007). Global observations of large oceanic eddies. s. *Geophysical Research Letters*, *34*, L15606. https://doi.org/10.1029/2007GL030812

Cleveland, W. S., & Devlin, S. J. (1988). Locally Weighted Regression: An Approach to Regression Analysis by Local Fitting. *Journal of American Statistical Association*, *83*(403), 596–610.

Collins, C. A., Margolina, T., Rago, T. A., & Ivanov, L. (2013). Looping RAFOS floats in the California Current System. *Deep Sea Research Part II*, *85*, 42–61. https://doi.org/10.1016/j.dsr2.2012.07.027

Dong, C., McWilliams, J. C., Liu, Y., & Chen, D. (2014). Global heat and salt transports by eddy movement. *Nature Communications*, *5*, 3294. https://doi.org/10.1038/ncomms4294

Dufois, F., Hardman-Mountford, N. J., Fernandes, M., Wojtasiewicz, B., Shenoy, D., Slawinski, D., et al.(2017). Observational insights into chlorophyll distributions of subtropical South Indian Ocean eddies. *Geophysical Research Letters*, *44*, 3255–3264. https://doi.org/10.1002/2016GL072371

Dufois, F., Hardman-Mountford, N. J., Greenwood, J., Richardson, A. J., Feng, M., Herbette, S., & Matear, R. (2014). Impact of eddies on surface chlorophyll in the South Indian Ocean. *Journal of Geophysical Research: Ocean*, *119*, 8061–8077. https://doi.org/10.1002/2014JC010164

Dufois, F., Hardman-Mountford, N. J., Greenwood, J., Richardson, A. J., Feng, M., & Matear, R. J. (2016). Anticyclonic eddies are more productive than cyclonic eddies in subtropical gyres because of winter mixing. *Science Advznces*, *2*(5), e1600,282–e1600,282. https://doi.org/10.1126/sciadv.1600282

Duncombe Rae, C. M., Garzoli, S. L., & Gordon, A. L. (1996). The eddy field of the southeast Atlantic Ocean: A statistical census from the Benguela Sources and Transports Project. *Journal of Geophysical Research*, *101*(C5), 11,949–11,964. https://doi.org/10.1029/95JC03360

Dunn, J., & Ridgway, K. (2002). Mapping ocean properties in regions of complex topography. *Deep Sea Research, Part I*, *49*(3), 591–604. https://doi.org/10.1016/S0967-0637(01)00069-3

Flierl, G. R. (1981). Particle motions in large-amplitude wave fields, *Geophyiscal & Astrophys. Fluid Dynamics*, *18*(1–2), 39–74. No

Garfield, N., Collins, C. A., Paquette, R. G., & Carter, E. (1999). Lagrangian Exploration of the California Undercurrent, 1992–95. *Journal of Physical Oceanography*, *29*(4), 560–583.

Gaube, P., Chelton, D. B., Strutton, P. G., & Behrenfeld, M. J. (2013). Satellite observations of chlorophyll, phytoplankton biomass, and Ekman pumping in nonlinear mesoscale eddies. *Journal of Geophysical Research. Ocean*, *118*, 6349–6370. https://doi.org/10.1002/2013JC009027

Gaube, P., McGillicuddy, D. J., Chelton, D. B., Behrenfeld, M. J., & Strutton, P. G. (2014). Regional variations in the influence of mesoscale eddies on near-surface chlorophyll. *Journal of Geophysical Research. Ocean*, *119*, 8195–8220. https://doi.org/10.1002/2014JC010111

Gill, A. E., & Niiler, P. P. (1973). The theory of the seasonal variability in the ocean. *Deep. Research Oceanographic Abstracts*, *20*(2), 141–177. https://doi.org/10.1016/0011-7471(73)90049-1

Hanawa, K., & Talley, L. (2001). Mode waters. In Siedler, G., Church, J., & Gould, J. (Eds.), *International Geophysics* (Vol. 77, pp. 373–386). New York City, NY: Elsevier. https://doi.org/10.1016/S0074-6142(01)80129-7

Hebert, D., Oakey, N., & Ruddick, B. (1990). Evolution of a Mediterranean Salt Lens: Scalar Properties. *Journal of Physical Oceanography*, *20*(9), 1468–1483.

Hogan, P. J., & Hurlburt, H. E. (2006). Why do intrathermocline eddies form in the Japan/East Sea? A modeling perspective, *Nav. Res. LAB STENNIS Sp. Cent. MS Oceanogr. DIV*, *31*(0704).

Iskandar, I., Sasaki, H., Sasai, Y., Masumoto, Y., & Mizuno, K. (2010). A numerical investigation of eddy-induced chlorophyll bloom in the southeastern tropical Indian Ocean during Indian Ocean Dipole 2006. *Ocean Dynamics*, *60*(3), 731–742. https://doi.org/10.1007/s10236-010-0290-6

Jayne, S. R., & Marotzke, J. (2002). The Oceanic Eddy Heat Transport*. *Journal of Physical Oceanography*, *32*(12), 3328–3345.

Jia, F., Wu, L., Lan, J., & Qiu, B. (2011b). Interannual modulation of eddy kinetic energy in the southeast Indian Ocean by Southern Annular Mode. *Journal of Geophysical Research*, *116*, C02029, https://doi.org/10.1029/2010JC006699

Jia, F., Wu, L., & Qiu, B. (2011a). Seasonal Modulation of Eddy Kinetic Energy and Its Formation Mechanism in the Southeast Indian Ocean. *Journal of Physical Oceanography*, *41*(4), 657–665. https://doi.org/10.1175/2010JPO4436.1

Kostianoy, A., & Belkin, I. (1989). A Survey of Observations on Intrathermocline Eddies in the World Ocean, *Elsevier Oceanography. Ser.*, vol. *50*, 821–841, https://doi.org/10.1016/S0422-9894(08)70223-X

L'Hégaret, P., Carton, X., Ambar, I., Ménesguen, C., Hua, B. L., Chérubin, L., et al. (2014). Evidence of Mediterranean Water dipole collision in the Gulf of Cadiz. *Journal of Geophysical Research. Ocean*, *119*, 5337–5359. https://doi.org/10.1002/2014JC009972

Li, C., Zhang, Z., Zhao, W., & Tian, J. (2017). A statistical study on the subthermocline submesoscale eddies in the northwestern Pacific Ocean based on Argo data. *Journal of Geophysical Research. Ocean*, *122*, 3586–3598. https://doi.org/10.1002/2016JC012561

McDowell, S. E., & Rossby, H. T. (1978). Mediterranean Water: An Intense Mesoscale Eddy off the Bahamas. *Science*, *202*, 1085–1087. https://doi.org/10.1126/science.202.4372.1085
McGillicuddy, D., & Robinson, A. (1997). Eddy-induced nutrient supply and new production in the Sargasso Sea. *Deep Sea Research, Part I Oceanogr. Res. Pap*, *44*(8), 1427–1450. https://doi.org/10.1016/S0967-0637(97)00024-1
McGillicuddy, D. J. (2015). Formation of Intrathermocline Lenses by Eddy Wind Interaction. *Journal of Physical Oceanography*, *45*(2), 606–612. https://doi.org/10.1175/JPO-D-14-0221.1
McGillicuddy, D. J., Anderson, L. A., Bates, N. R., Bibby, T., Buesseler, K. O., Carlson, C. A., et al. (2007). Eddy/Wind Interactions Stimulate Extraordinary Mid-Ocean Plankton Blooms. *Science*, (80-.)., *316*(5827), 1021–1026. https://doi.org/10.1126/science.1136256
Mcwilliams, J. C. (1985). Submesoscale Coherent Vortices in the Ocean. *Rev.iew of Geophysics*, *23*(2), 165–182.
Morrow, R., Birol, F., Griffin, D., & Sudre, J. (2004). Divergent pathways of cyclonic and anti-cyclonic ocean eddies. *Geophysical Research Letters*, *31*, L24311, https://doi.org/10.1029/2004GL020974
Nauw, J. J., van Aken, H. M., Lutjeharms, J. R. E., & de Ruijter, W. P. M. (2006). Intrathermocline eddies in the Southern Indian Ocean. *Journal of Geophysical Research*, *111*, C03006, https://doi.org/10.1029/2005JC002917
O'Connor, B. M., Fine, R. A., & Olson, D. B. (2005). A global comparison of subtropical underwater formation rates. *Deep Sea Research, Part I*, *52*(9), 1569–1590. https://doi.org/10.1016/j.dsr.2005.01.011
Owens, W. B., & Wong, A. P. (2009). An improved calibration method for the drift of the conductivity sensor on autonomous CTD profiling floats by θ–S climatology. *Deep Sea Research, Part I*, *56*(3), 450–457. https://doi.org/10.1016/j.dsr.2008.09.008
Palastanga, V., van Leeuwen, P. J., Schouten, M. W., & de Ruijter, W. P. M. (2007). Flow structure and variability in the subtropical Indian Ocean: Instability of the South Indian Ocean Countercurrent. *Journal of Geophysical Research*, *112*, C01001. https://doi.org/10.1029/2005JC003395
Pelland, N. A., Eriksen, C. C., & Lee, C. M. (2013). Subthermocline Eddies over the Washington Continental Slope as Observed by Seagliders, 2003–2009. *Journal of Physical Oceanography*, *43*(10), 2025–2053. https://doi.org/10.1175/JPO-D-12-086.1
Penven, P., Halo, I., Pous, S., & Marié, L. (2014). Cyclogeostrophic balance in the Mozambique Channel. *Journal of Geophysical Research. Ocean*, *119*, 1054–1067. https://doi.org/10.1002/2013JC009528
Ponsoni, L., Aguiar-González, B., Maas, L. R., van Aken, H. M., & Ridderinkhof, H. (2015). Long-term observations of the East Madagascar Undercurrent. *Deep Sea. Research, Part I*, *100*, 64–78. https://doi.org/10.1016/j.dsr.2015.02.004
Ponsoni, L., Aguiar-González, B., Ridderinkhof, H., & Maas, L. R. M. (2016). The East Madagascar Current: Volume Transport and Variability Based on Long-Term Observations*. *Journal of Physical Oceanography*, *46*(4), 1045–1065. https://doi.org/10.1175/JPO-D-15-0154.1
Qiu, B., & Chen, S. (2005). Eddy-Induced Heat Transport in the Subtropical North Pacific from Argo, TMI, and Altimetry Measurements. *Journal of Physical Oceanography*, *35*(4), 458–473. https://doi.org/10.1175/JPO2696.1
Quartly, G., Buck, J., Srokosz, M., & Coward, A. (2006). Eddies around Madagascar The retroflection re-considered. *Journal of Marine Systems*, *63*(3–4), 115–129. https://doi.org/10.1016/j.jmarsys.2006.06.001
Ridgway, K. R., Dunn, J. R., & Wilkin, J. L. (2002). Ocean Interpolation by Four-Dimensional Weighted Least Squares–Application to the Waters around Australasia. *Journal of Atmospheric and Oceanic Technology*, *19*(9), 1357–1375.
Riser, S. C., Freeland, H. J., Roemmich, D., Wijffels, S., Troisi, A., Belbéoch, M., et al. (2016). Fifteen years of ocean observations with the global Argo array. *Nature Clim.aticChange*, *6*(2), 145–153. https://doi.org/10.1038/nclimate2872
Robinson, A. (1983). Overview and summary of eddy science. in *Eddies Mar. Sci.* (pp. 3–15). Berlin, Heidelberg: Springer.
Roullet, G., Capet, X., & Maze, G. (2014). Global interior eddy available potential energy diagnosed from Argo floats. *Geophysical. Research. Letters*, *41*, 1651–1656. https://doi.org/10.1002/2013GL059004
Sangrà, P., Pascual, A., Rodríguez-Santana, Á., Machín, F., Mason, E., et al. (2009). The Canary Eddy Corridor: A major pathway for long-lived eddies in the subtropical North Atlantic. *Deep Sea Research, Part I*, *56*(12), 2100–2114. https://doi.org/10.1016/j.dsr.2009.08.008
Schlax, M. G., & Chelton, D. B. (2016). The'' Growing Method'' of Eddy Identification and Tracking in Two and Three Dimensions Corvallis, OR: College of Earth, Ocean and Atmospheric Sciences, Oregon State University.
Shapiro, G., & Meschanov, S. (1991). Distribution and spreading of Red Sea Water and salt lens formation in the northwest Indian Ocean. *Deep Sea Research, Part A*, *38*(1), 21–34. https://doi.org/10.1016/0198-0149(91)90052-H
Siedler, G., Rouault, M., & Lutjeharms, J. R. (2006). Structure and origin of the subtropical South Indian Ocean Countercurrent. *Geophysical Research Letters 33* L24609, https://doi.org/10.1029/2006GL027399
Souza, J. M. A. C., de Boyer Montégut, C., Cabanes, C., & Klein, P. (2011). Estimation of the Agulhas ring impacts on meridional heat fluxes and transport using ARGO floats and satellite data. *Geophysical Research Letters*, *38*, https://doi.org/10.1029/2011GL049359
Thomas, L. N. (2008). Formation of interthermocline eddies at ocean fronts by wind-driven detruction of potential vorticity. *Dynamics of Atmospheres and Oceans*, *45*, 252–273.
Thomsen, S., Kanzow, T., Krahmann, G., Greatbatch, R. J., Dengler, M., & Lavik, G. (2016). The formation of a subsurface anticyclonic eddy in the Peru-Chile Undercurrent and its impact on the near-coastal salinity, oxygen, and nutrient distributions. *Journal of Geophysical Research. Ocean*, *121*, 476–501. https://doi.org/10.1002/2015JC010878
Tomczak, M., & Godfrey, J. S. (1994). Regional Oceanography: An Introduction. *Elsevier Sci. LTD*, *660*, 10,591–5153.
Volkov, D. L., Lee, T., & Fu, L. L. (2008). Eddy-induced meridional heat transport in the ocean. *Geophysical Research Letters*, *35*, 1–5. https://doi.org/10.1029/2008GL035490
Williams, S., Petersen, M., Bremer, P-T., Hecht, M., Pascucci, V., Ahrens, J.,et al. (2011). Adaptive Extraction and Quantification of Geophysical Vortices. *IEEE Transactions on Visualization and Computer Graphics*, *17*(12), 2088–2095.
Wong, A. P. S., Johnson, G. C., & Owens, W. B. (2003). Delayed-Mode Calibration of Autonomous CTD Profiling Float Salinity Data by θ–S Climatology* *Journal of Atmospheric and Oceanis Technology*, *20*(2), 308–318.
Yang, G., Wang, F., Li, Y., & Lin, P. (2013). Mesoscale eddies in the northwestern subtropical Pacific Ocean: Statistical characteristics and three-dimensional structures. *Journal of Geophysical Research. Ocean*, *118*, 1906–1925. https://doi.org/10.1002/jgrc.20164
Yang, G., Yu, W., Yuan, Y., Zhao, X., Wang, F., Chen, G., et al. (2015). Characteristics, vertical structures, and heat/salt transports of mesoscale eddies in the southeastern tropical Indian Ocean. *Journal of Geophysical Research. Ocean*, *120*, 6733–6750. https://doi.org/10.1002/2015JC011130
Zhang, Z., Li, P., Xu, L., Li, C., Zhao, W., Tian, J., & Qu, T. (2015). Subthermocline eddies observed by rapid-sampling Argo floats in the subtropical northwestern Pacific Ocean in Spring 2014. *Geophysical Research Letters*, *42*, 6438–6445. https://doi.org/10.1002/2015GL064601
Zhang, Z., Wang, W., & Qiu, B. (2014). Oceanic mass transport by mesoscale eddies. *Science*, (80-.)., *345*(6194), 322–324. https://doi.org/10.1126/science.1252418
Zheng, S., Du, Y., Li, J., & Cheng, X. (2015). Eddy characteristics in the South Indian Ocean as inferred from surface drifters. *Ocean Science*, *11*(3), 361–371. https://doi.org/10.5194/os-11-361-2015